THE ASTROPHYSICAL JOURNAL, 611:494–516, 2004 August 10

THE (IN)STABILITY OF PLANETARY SYSTEMS

RORY BARNES AND THOMAS QUINN
Department of Astronomy, University of Washington, Box 351580, Seattle, WA 98195-1580; rory@astro.washington.edu, rq@astro.washington.edu
Received 2004 January 12; accepted 2004 March 19

ABSTRACT

We present results of numerical simulations that examine the dynamical stability of known planetary systems, a star with two or more planets. First we vary the initial conditions of each system on the basis of observational data. We then determine regions of phase space that produce stable planetary configurations. For each system we perform 1000 $\sim 10^6$ yr integrations. We examine υ And, HD 83443, GJ 876, HD 82943, 47 UMa, HD 168443, and the solar system. We find that the resonant systems, two planets in a first-order mean motion resonance (HD 82943 and GJ 876) have very narrow zones of stability. The interacting systems, not in first-order resonance, but able to perturb each other (υ And, 47 UMa, and the solar system), have broad stable regions. The separated systems, two planets beyond 10:1 resonance (we examine only HD 83443 and HD 168443) are fully stable. We find that the best fits to the interacting and resonant systems place them very close to unstable regions. The boundary in phase space between stability and instability depends strongly on the eccentricities and (if applicable) the proximity of the system to perfect resonance. Furthermore, we also find that the longitudes of periastron circulate in chaotic systems but librate in regular systems. In addition to 10^6 yr integrations, we also examined stability on $\sim 10^8$ yr timescales. For each system we ran $\sim$10 long-term simulations, and find that the Keplerian fits to these systems all contain configurations that are regular on this timescale.

Subject headings: celestial mechanics — methods: *n*-body simulations — planetary systems

1. INTRODUCTION

By 2003 September 13 planetary systems had been discovered (including our own solar system). The extrasolar planetary systems (ESPSs) are, possibly because of observational biases, markedly different from our own in several ways. In our solar system (SS) the Jovian-mass planets all orbit at distances larger than 5 AU, and on nearly circular orbits ($e \lesssim 0.05$). ESPSs, on the other hand, contain giant planets in a wide range of distances and eccentricities; some are 10 times closer to their primary than Mercury, and others orbit with eccentricities larger than 0.5. In this paper we attempt to categorize these systems dynamically, constrain the errors of the orbital parameters, compare our SS to ESPSs, explore the long-term stability of each planetary system, and determine the mechanism(s) that maintain stability.

We examine these systems through numerical simulations. The integrations begin with slightly different initial conditions in order to probe observationally allowed configurations. This exploration of parameter space permits a quantitative measure of the stability of each system and hence predicts which distribution of orbital elements will most likely result in a stable system. In addition, a comparison of stability between systems may reveal which elements are most critical to the stability of planetary systems in general.

A quick inspection of the known systems reveals three obvious morphological classifications: resonant, interacting, and separated. Resonant systems contain two planets that occupy orbits very close to a 2:1 mean motion resonance. A 3:1 system, 55 Cnc (Marcy et al. 2002), has been announced, but its dynamics will not be examined here. Interacting systems contain planets that are not in mean motion resonance but are separated by less than a 10:1 ratio in orbital period. These systems are not dynamically locked, but the planets perturb each other. The SS falls into this category. The final classification is systems in which the (detected) planets' orbits are beyond the 10:1 resonance. These planets are most likely dynamically decoupled (i.e., they can be modeled as planets on Kepler orbits); however, some of these separated systems warrant investigation.

We examine planetary systems on two different timescales. First, we explore parameter space in 10^6 yr integrations. For these simulations we vary initial conditions to determine stable regions within the observed errors. Second, we continue several stable simulations for an additional 10^8–10^9 yr. From these runs we then learn how robust the predicted stable regions are, and we also determine the mechanisms that lead to stability. Specifically we evaluate the hypothesis that some stable system require secular resonance locking.

In many ways this paper performs the direct analysis that is approximated by MEGNO (Cincotta & Simó 2000; see also Robutel & Laskar 2001; Michtchenko & Ferraz-Mello 2001; Goździewski 2002). MEGNO searches parameter space for chaotic and periodic regions. Our simulations show that to first-order MEGNO's results do uncover unstable regions. In general, however, chaotic systems can be stable for at least 10^9 yr, as shown below. Our SS also shows chaos on all timescales (for a complete review, see Lecar et al. 2001); therefore direct *N*-body integrations are the best available method for determining stability.

This work represents the largest coherent study of planetary system dynamics to date. Our simulations show that the true configurations of most planetary systems are constrained by just a few orbital elements (or ratios of elements) and that stable regions can be identified with integrations on the order of 10^6 yr. We also find that stability, as well as constraints on stability, are correlated with morphology. Resonant system stability depends strongly on the ratio of the periods, interacting systems depend on eccentricities, and separated systems are stable.

This paper is structured as follows. In § 2 we describe the generation of initial conditions and the integration technique, and we introduce the concept of a stability map. In § 3 we analyze the results of the resonant systems HD 82943 and GJ 876. In § 4 we examine the interacting systems of 47 UMa, υ And, and the SS. In § 5 the separated systems, specifically HD 168443 and HD 83443, are discussed briefly. In § 6 we summarize the results of §§ 3–5. In § 7 we discuss possible formation scenarios and inconsistencies between this work and other work on planetary systems. Finally, in § 8 we draw general conclusions and suggest directions for future work.

2. NUMERICAL METHODS

In this section we outline the techniques used to perform and analyze these simulations. This paper follows the example of Barnes & Quinn (2001, hereafter Paper I). First we describe how the initial conditions of each of the short-term simulations are determined. In § 2.2 we describe our integration method. Finally in § 2.3 we describe a convenient way to visualize the results of these simulations, the stability map.

2.1. *Initial Conditions*

In order to explore all of parameter space we must vary six orbital elements (the period P, the eccentricity e, the longitude of ascending node Ω, the longitude of periastron ϖ, the inclination i, and the time of periastron passage $T_{\rm peri}$) and every mass in the system. The period and the semimajor axis a are related by Kepler's third law. The argument of pericenter, ω, is the difference between ϖ and Ω.

For each system we perform 1000 simulations, each with different initial conditions. Orbital elements that are easily determined via the Doppler method (P, e, ϖ, $T_{\rm peri}$) are varied about a Gaussian centered on the nominal value, with a standard deviation equal to the published error. We do not permit any element to be more than 5 σ from the mean. For the i and Ω elements, flat distributions in the ranges $0° < i < 5°$ and $0 < \Omega < 2\pi$ were used. Note that this distribution of i and Ω permits a maximum mutual inclination of 10°. These randomized orbital elements are relative to the fundamental plane.

The Doppler method of detection does not produce a normal error distribution. As Konacki & Maciejewski (1999) show, the error in eccentricity can have a large tail toward unity. However, their method, or other statistical methods, such as bootstrapping, require all the observational data (including reflex velocity errors) to determine the shape of this error curve. As not all the observations of multiplanet systems have been published, we are forced to use a normal distribution in order for comparison between systems to be meaningful. We therefore encourage that all the observational data be published, as some of the results presented here (specifically comparing the percentage of simulations that survived) are less meaningful because we are unable to accurately estimate the error distributions of the orbital elements. For completeness we also vary the primaries' masses, M_*, based on other observations (generally determined via spectral fitting). However, as the stars are all at least 100 times more massive than their planetary companions, the slight variations in primary mass should not affect stability.

The masses of the planets are determined by the following relation

$$m = \frac{m_{\rm obs}}{|\sin[\cos^{-1}(\sin i)\cos\Omega]|}, \tag{1}$$

where m is the true mass of the planet and $m_{\rm obs}$ is the observed minimum mass. By varying the mass this way, we account for all possible orientations and connect the inclination of the system to its inclination in the sky. Note that this scheme requires the azimuthal angles in the planetary systems to be measured from the line of sight.

2.2. *Integration*

With initial conditions determined the systems were then integrated with the RMVS3 code from the SWIFT suite of programs[1] (Levison & Duncan 1994). This code uses a symplectic integration scheme to minimize long-term errors, as well as regularization, to handle close approaches. The initial time step, Δt is approximately 1/30 of the orbital time of the innermost planet. In order to verify the accuracy of the integrations, the maximum change in energy, ϵ, permitted was 10^{-4}. We define ϵ as

$$\epsilon = \frac{\max|E_i - E_0|}{E_0}, \tag{2}$$

where E_i represents an individual measurement of the energy during the simulation and E_0 is the energy at time 0. There are two reasons for using this threshold in ϵ. First, as the integration scheme is symplectic, no long-term secular changes will occur, so high precision is not required. Second, the simulations needed to be completed in a timely manner. If a simulation did not meet this energy conservation criterion, it was rerun with the time stamp reduced by a factor of 10. The minimum time stamp we used was $P_{\rm inner}/3000$. Despite this small time stamp, a few simulations did not conserve energy and were discarded, except that they were incorporated into the errors. Errors and error bars include information from unconserved simulations. Simulations that fail to conserve energy would most likely be labeled as unstable, since the failure of energy conservation undoubtedly results from a close encounter between two bodies, which usually results in an ejection. Therefore the estimates for stability in the systems presented here should be considered *upper* limits.

Throughout this paper we adopt the nomenclature of the discovery papers (planets have been labeled b, c, d, etc., with order in the alphabet corresponding to order of discovery). We will also introduce another scheme based on mass. Planets will be subscripted with a 1, 2, 3, etc., in order of descending mass. This new scheme is more useful in discussing the dynamics of the system.

The short-term simulations are integrated until one of the following criteria is met: (1) The simulation ejects a planet. Ejection is defined as the osculating eccentricity of one planet reaching, or exceeding unity. (2) The simulation integrates to completion at time τ. For these simulations, τ is defined as

$$\tau \equiv 2.8 \times 10^5 P_1, \tag{3}$$

or 280,000 times the period of the most massive planet. This choice corresponds to 10^6 yr for the υ And system, as was simulated in Paper I.

If a system ends without ejection, then the stability of the system must be determined. There are several possible definitions of stability. In Paper I a system was stable if the osculating eccentricity of each companion remained below 1 for the duration of the simulation. The most obvious flaw in this definition is that a planet could suffer a close approach and be thrown out to a bound orbit at some arbitrarily large distance.

[1] SWIFT is publicly available at http://k2.space.swri.edu/~hal/swift.html.

TABLE 1
Initial Conditions for Resonant Systems

System	Planet	Mass (M_J)	Period (day)	Eccentricity	Longitude of Periastron (deg)	Time of Periastron (JD)
GJ 876	c	0.56	30.12 ± 0.02	0.27 ± 0.04	330.0 ± 12.0	2450031.4 ± 1.2
	b	1.89	61.02 ± 0.03	0.10 ± 0.02	333.0 ± 12.0	2450045.2 ± 1.9
HD 82943	b	0.88	221.6 ± 2.7	0.54 ± 0.05	138 ± 13	2451630.9 ± 5.9
	c	1.63	444.6 ± 8.8	0.41 ± 0.08	96 ± 7	2451620.3 ± 12.0

Such a system would bear no resemblance to the observed system and hence should be labeled unstable. Here we adopt a more stringent definition, namely, that the semimajor axes of all companions cannot change by more than a factor of 2. Changes in semimajor axis represent a major perturbation to the system; therefore this second cut is conservative and eliminates only systems that expel a planet to large distances without fully ejecting it.

In addition to these short-term simulations, we completed simulations to explore longer term stability ($\sim 10^8$ yr). For each system we ran $\sim$10 simulations, chosen to cover a wide range of stable parameter space. For these runs we started with the final conditions of stable configurations and continued them. These simulations therefore give us a handle on how the system is likely to evolve on timescales closer to its age ($\sim 10^9$ yr). Those systems that survived these longer runs are the best comparisons to the true system. Hence they are the best simulations for determining the factors that lead to planetary system stability.

There are two notable problems with this methodology. First, we ignore the effects of general relativity, which may be important in some systems, specifically GJ 876 and υ And. General relativity was included in our treatment of υ And in Paper I. In Paper I the innermost planet had a negligible effect on the system, and we presume that general relativity will continue to be unimportant for the systems studied here. Second, we treat all particles as point masses. This is again especially troublesome for GJ 876 and υ And, because of their proximity to their (presumably) oblate primaries. The sphericity of the stars also prohibits any tidal circularization of highly eccentric planets (Rasio et al. 1996). This may artificially maintain large planetary eccentricities and increase the frequency of close encounters. However, the eccentricities must become very large for this effect to become appreciable. We therefore assume that this phenomenon will not adversely affect our results. Ignoring these two issues should impact the results minimally while speeding up our simulations considerably.

2.3. *Stability Maps*

When analyzing the simulations, it is useful to visualize the results in a stability map. In general a stability map is a three-dimensional representation of stability as a function of two parameters. In resonant systems, we find that several parameters determine stability. The most important is the ratios of the periods of the two resonant planets, which we will call R:

$$R \equiv \frac{P_{\rm outer}}{P_{\rm inner}}. \tag{4}$$

In coupled systems, e_1 and e_2 are the relevant parameters. The advantage to this visualization is that boundaries between stability and instability are easily identified.

The disadvantage of this form of visualization is that if the range of parameter space is not uniformly sampled (as it is here), we cannot visualize of the errors. It is therefore important to bear this disadvantage in mind. At the edges of stability maps, the data are poorly sampled and the information at the edges should largely be ignored. To aid the visualization we have smoothed the maps. If a bin contained no data, then it was given the weighted mean of all adjacent bins, including diagonal bins. This methodology can produce some misleading features in the stability maps. Most notable are tall spikes or deep depressions in sparsely sampled regions. We comment on these types of errors where appropriate.

The procedure as outlined overestimates the size of stable regions in two important ways. First, the integration times are generally less than 0.1% of the systems' true ages. As is shown throughout this paper, instability can arise at any timescale. Therefore, the stability zone will continue to shrink as the system evolves. Second, we have chosen a very generous cut in semimajor axis space. Other studies permit Δa to be no larger than 10% (Chiang et al. 2001). Lowering this variation would undoubtedly also constrict stability zones.

3. RESONANT SYSTEMS

Two systems with orbital periods in 2:1 mean motion resonance have been detected: HD 82943[2] and GJ 876 (Marcy et al. 2001a). Table 1 lists the orbital elements and errors for the resonant systems. For now we do not examine the 3:1 55 Cnc system. The current best Keplerian fit to the observations put HD 82943 and GJ 876 just beyond perfect resonance. These planets all occupy high-eccentricity orbits and hence have wide resonance zones. Simulations of these systems show that stability is highly correlated with the ratio of the periods, R, and to a lesser degree on e_1. These systems have the smallest stable regions as less than 20% of simulations survived to τ.

3.1. *HD 82943*

Two planets orbit the $1.05 \pm 0.05\ M_\odot$ G0 star (Santos et al. 2000) HD 82943 at semimajor axis distances of 0.73 and 1.16 AU. Planet b is the inner and less massive, c, the outer and more massive. Other research on this system has shown that this system is most likely stable when it is in both a mean motion and apsidal resonance (Goździewski & Maciejewski 2001; Ji et al. 2003 also examined this system). They found that the system is most likely to be stable in perfect resonance. These simulations must run for 340,830 yr, $\tau_{\rm HD\ 82943}$. The long-term simulations were run for 100 million years.

For this system we find that 18.8% ± 4.3% of the trials were unperturbed to $\tau_{\rm HD\ 82943}$, 17.8% survived for 10^6 yr, and 4.5% failed to conserve energy. We determine the error in this number by considering the 1000 trials as 10 suites of 100 simulations,

[2] See http://obswww.unige.ch/~udry/planet/hd82943syst.html.

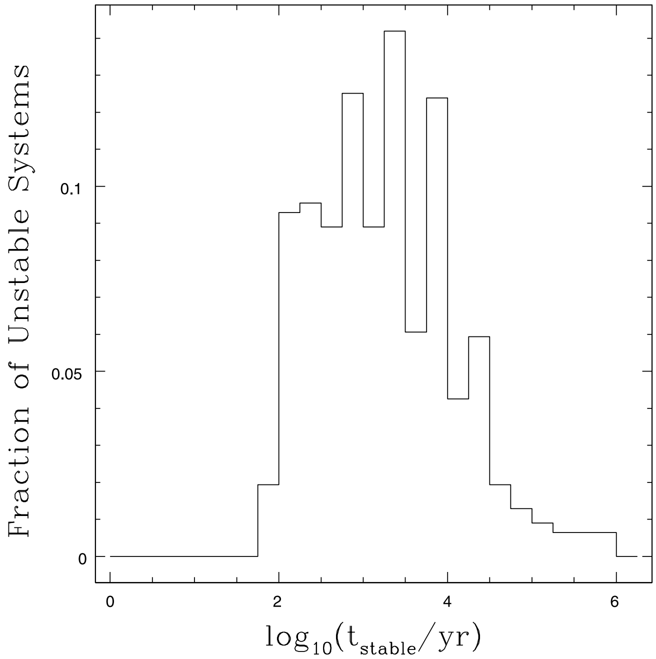

FIG. 1.—Distribution of instability times for unstable configurations of HD 82943. Most unstable systems survive for just 10^2–10^4 yr before perturbations change a semimajor axis by more than a factor of 2.

and calculate the standard deviation of these 10 data points. Figure 1 shows the instability rate to 10^6 yr. Most unstable simulations break our stability criterion within 10^4 yr, but others survived more than 900,000 yr before ejecting a planet. The asymptotic falloff to 10^6 yr implies that we have found most unstable configurations. In 91.3% of the trials, planet b, the inner and less massive planet, was ejected/perturbed. In order to check the simulations, Figure 2 plots the rate of survival as a function of energy conservation. From this figure it appears that our limit of 10^{-4} is reasonable, since there appears to be no trend in stability as a function of energy conservation. The

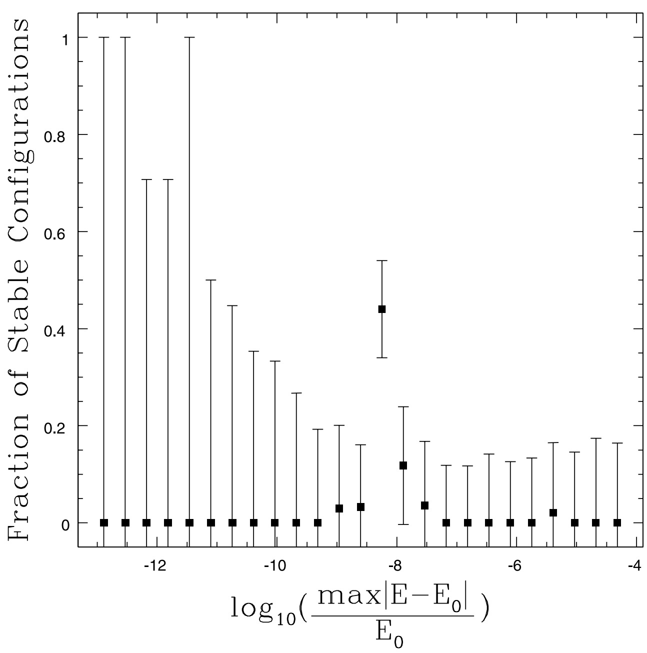

FIG. 2.—Survival rate as a function of energy conservation for HD 82943. The lack of a trend implies that the results for the system are accurate.

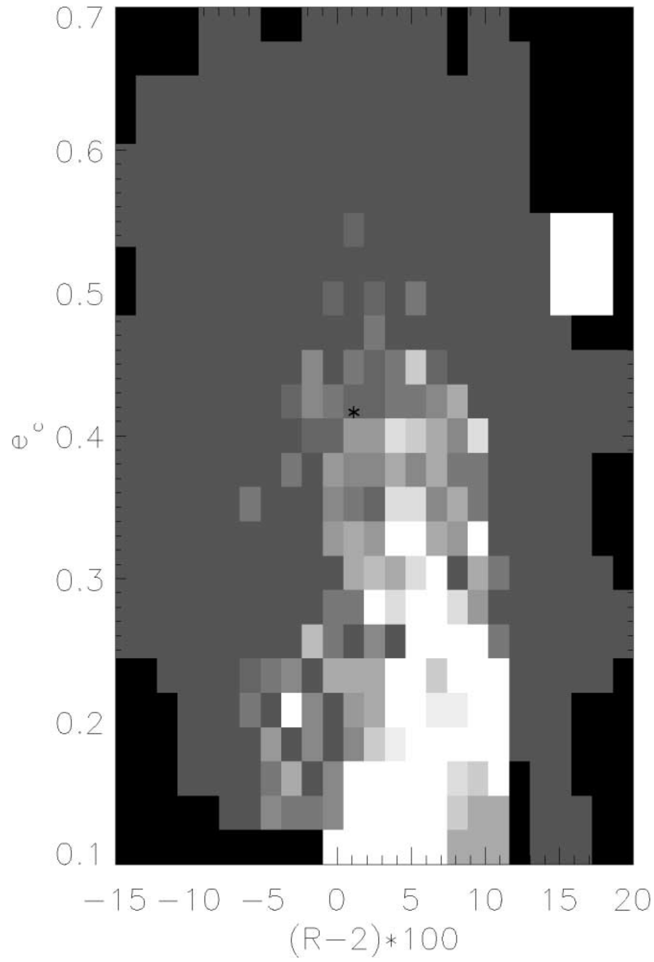

FIG. 3.—R-e_c stability map for HD 82943. The asterisk represents the best fit to the system as of 2002 July 31. The data are most accurate closer to the asterisk. The system shows a clear boundary in phase space between unstable (*dark gray*) and stable (*white*) regions. Black represents unsampled data. The stable region at $R = 2.15$, $e_c = 0.52$ is a bin in which 1 of 1 trials survived.

spike in survivability at 10^{-8} corresponds to regular orbits that were stable for our initial choice of Δt. The lack of a trend with energy conservation (specifically survival probability increasing with decreasing ϵ), implies our cutoff value of ϵ is stringent enough.

Stability in this system is correlated with R, e_c, ΔM, and $\Delta\varpi$, where ΔM is the difference in mean anomaly and $\Delta\varpi$ is the difference in initial longitude of periastron. Slightly beyond perfect resonance is the preferred state for this system. This system also requires the eccentricity of planet c to remain below 0.4. These features are shown in Figures 3 and 4. In these gray-scale images, black represents unsampled regions, the darkest gray marks regions in which no configurations survived, grades of stability are denoted by lighter shades of gray, and white is fully stable. As with most stability maps in this paper, the outer 2–3 grid points should be ignored. In Figure 3 the R-e_c stability map, the large "plateau" at low e, is therefore poorly sampled, as is the island at $R = 2.15$, $e_c = 0.52$. The most striking feature of this figure is that the best fit to the system, the asterisk, places it adjacent to stability. If R is changed by less that 5%, the system has no chance of surviving even 1 million years. This map shows that the current fit to the system is not correct. However, the elements do not need to change by much (specifically e_c needs to be slightly lower) for the system to have a chance at stability.

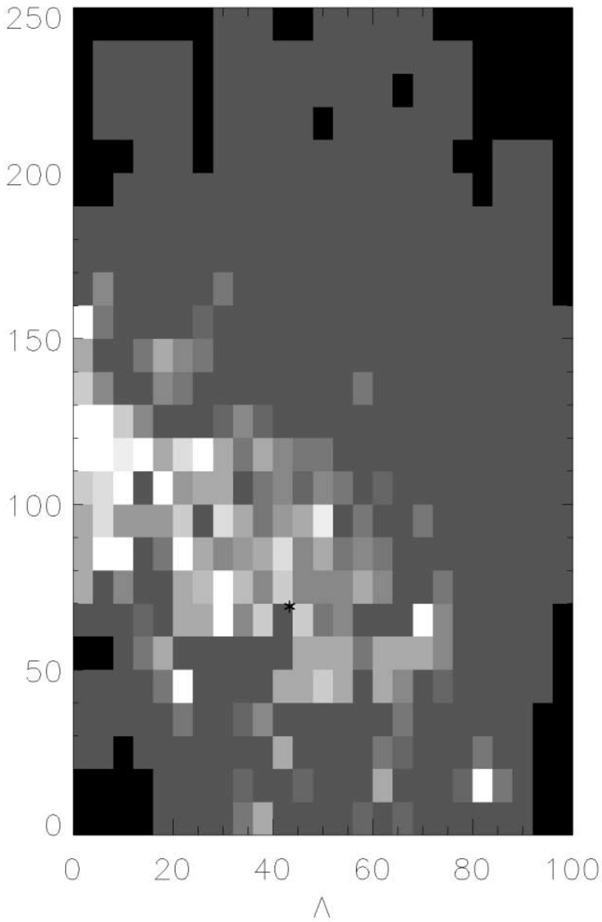

FIG. 4.—Λ-ΔM stability map for HD 82943. The asterisk represents the best fit to the system as of 2002 July 31. The data are most accurate closer to the asterisk. Stability appears to follow the line represented by eq. (6). Note, however, that the system is also constrained to $\Lambda \leq 75^\circ$ and $\Delta M \geq 30^\circ$. The island at $\Lambda = 80^\circ$, $\Delta M = 20^\circ$ is a bin in which 1 of 1 trials survived.

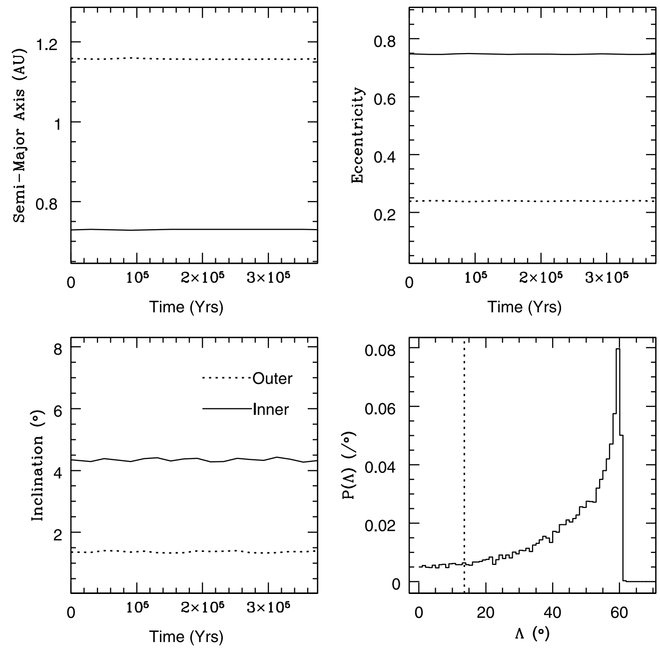

FIG. 5.—Orbital evolution of HD 82943−348, a stable, regular configuration. The data here are smoothed over a 20,000 yr interval. *Top left:* The evolution in semimajor axis. The planets show slight variations due to resonant interactions. *Top right:* The eccentricities oscillate with a 700 yr period, with $0.62 \leq e_b \leq 0.85$ and $0.05 \leq e_c \leq 0.45$. This short timescale is not visible in this plot. *Bottom left:* The inclinations experience oscillations on a 2100 yr timescale, again too short to be visible in this plot. The ranges of inclination are $1^\circ \leq i_b \leq 7^\circ$ and $0^\circ \leq i_c \leq 3^\circ$. *Bottom right:* From this distribution function we see the lines of node librate harmonically with an amplitude of 60°. The dashed vertical line represents Λ_0, the initial value of Λ.

The system also shows dependence on mean anomaly and longitude of periastron. Because of the symmetry of ellipses, we will introduce a new variable, Λ, defined as

$$\Lambda \equiv \begin{cases} |\varpi_1 - \varpi_2|, & \Lambda < \pi, \\ 360 - |\varpi_1 - \varpi_2|, & \Lambda > \pi, \end{cases} \tag{5}$$

where the subscripts merely represent two different planets, b and c, for this system. The order is unimportant, as we are concerned only with the magnitude of this angle. In Figure 4 the Λ-ΔM stability map is presented. The asterisk marks the best fit to the system. Stability seems to follow a line represented by

$$\Delta M = \frac{4}{3}\Lambda + 120 = \frac{4}{3}\left(\Lambda + \frac{\pi}{2}\right). \tag{6}$$

This relation is purely empirical. As is shown in the following sections, this interdependency is unusual for extrasolar planetary systems. Similar plots of ΔM or Λ versus R show the same R dependence as in Figure 3. Therefore R is clearly the most important parameter in this system, but these other three also play an important role in the system. As more observations of the system are made, HD 82943 should fall into the region defined by $1.95 \leq R \leq 2.1$, $e_c < 0.4$, and equation (6).

HD 82943 shows a wide range of dynamics. Some examples of these are shown in Figures 5–8. The initial conditions

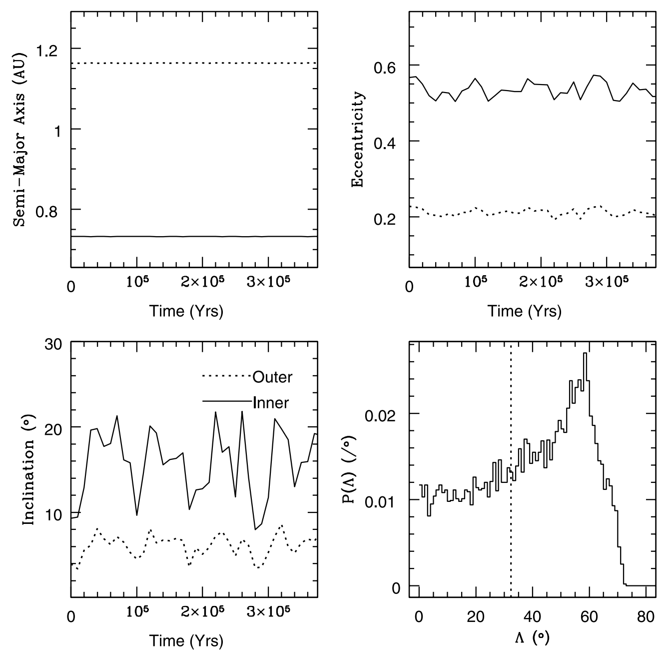

FIG. 6.—Orbital evolution of HD 82943−382, a stable, chaotic configuration of HD 82943. The data are averaged on a 10,000 yr interval. *Top left:* The evolution in semimajor axis. The planets clearly never experience a close encounter. *Top right:* The eccentricities experience low-amplitude (≈13%) chaotic oscillations. *Bottom left:* The inclinations initially jump to large values and experience large amplitude (≈70%) fluctuations. *Bottom right:* The Λ distribution function suggests that Λ is generally librating but that there are chaotic fluctuations superposed on this motion. The dashed vertical line is the value of Λ_0.

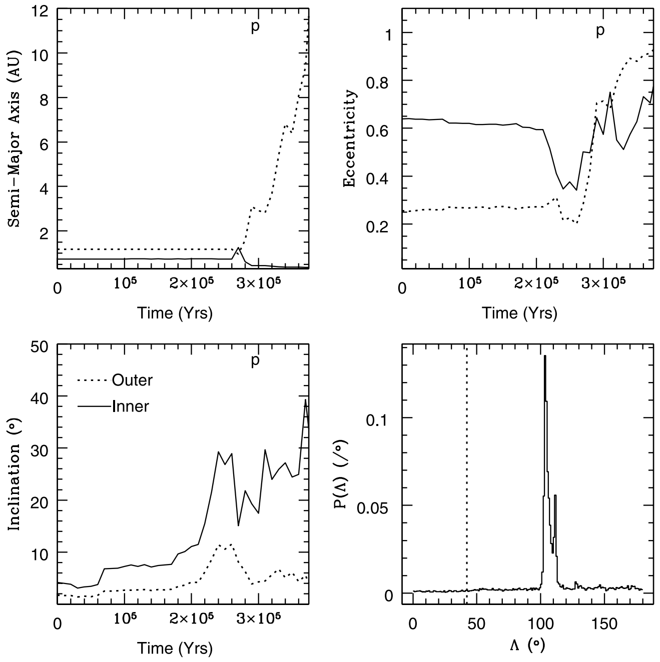

FIG. 7.—Orbital evolution of HD 82943−216, the perturbation of HD 82943c. The parameters are averaged on 10,000 yr intervals. *Top left:* The planets' semimajor axes are stable and show no signs of close encounters until 260,000 yr. At this point planet c actually crosses b's orbit. This initial encounter leads to more encounters as a_c reaches 3 AU by 280,000 yr, tripping the criterion for instability. *Top right:* The eccentricities experience secular change until 210,000 yr. The system then moves into a lower eccentricity state. The eccentricity then grows to large values and remain at their final values for another 700,000 yr. *Bottom left:* As with eccentricity the inclinations show slow secular change until 210,000 yr. The inclinations then leap up to 30° in the case of planet b. *Bottom right:* The Λ distribution function is the sum of two motions: the preperturbation motion is circulation, the post-perturbation motion is fixed close to 110°. The dashed line represents Λ_0. Note that this distribution is for the full 10^6 yr integration.

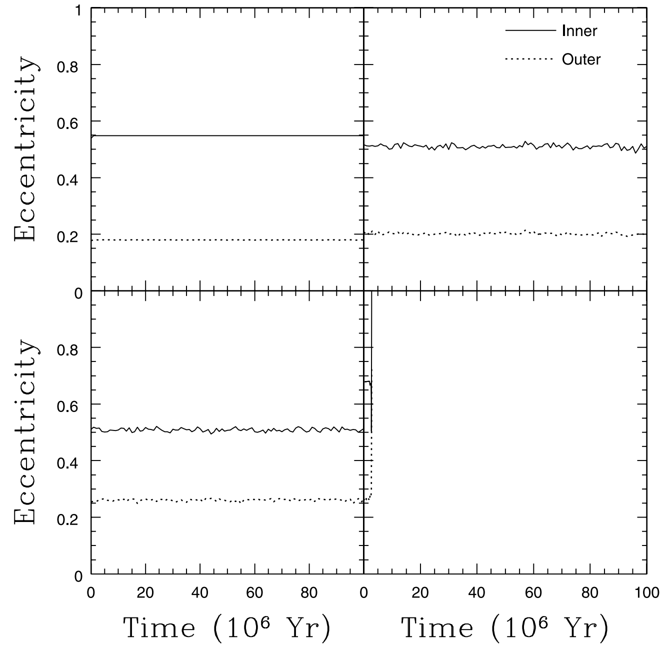

FIG. 8.—Long-term simulations of the HD 82943 system. These data are averages over 50,000 yr intervals. *Top left:* Evolution of HD 82943−035. An example in which the system is regular. *Top right:* Evolution of HD 82943−021, an example of chaotic evolution. *Bottom left:* Evolution of HD 82943−000, another example of chaotic motion. *Bottom right:* Evolution of HD 82943−032. A chaotic system which ejects planet b after 2.4 million years ($7\tau_{\rm HD\ 82943}$).

of these systems are presented in Table 2. Figure 5 is an example of the evolution of a regular system, HD 82943−348, which shows no evidence of chaos. Note that instead of $\Lambda(t)$, we present the distribution function of Λ, $P(\Lambda)$, the probability of Λ, versus Λ. This representation of Λ shows that the motion is like that of a harmonic oscillator; the longitudes of periastron are librating with an amplitude of 60°.

Figure 6 (HD 82943−382) is a stable case which is clearly chaotic. Although the eccentricities remain close to their initial values, the inclinations jump to large values quickly. Note that Λ never exceeds 75°, but its motion is slightly nonharmonic, another indication of chaos.

In Figure 7 the orbital evolution of simulation HD 82943−216 is shown. This system perturbed planet c after 280,000 yr, and, despite the high eccentricities the system reached (>0.75 for both planets), remained bound for 10^6 yr. The inclinations also show large growth. Although initially $\Lambda = 41°$, the system appears to become locked at just over 100°. This is misleading since this is the Λ distribution for the full 10^6 yr. It is actually the superposition of two modes. Initially, until perturbation at 280,000 yr, the system circulates with a slight preference toward antialignment. However, after the perturbation the system becomes locked at $\Lambda \approx 100°$. Although not shown, after these initial perturbations the system settles down to a configuration in which $a_b \approx 0.344$ AU, $e_b \approx 0.79$ and $a_c \approx 2400$ AU, $e_c \approx 0.99$. At this semimajor axis the period of the orbit is over 115,000 yr, so this system should not be considered locked as the planet has made less than 10 periastron passages since being flung to such a large semimajor axis.

We ran 10 simulations for 10^8 yr. The initial conditions and results of these simulations are presented in Table 3. The eccentricity evolution of four simulations is shown in Figure 8. These simulations show that some configurations are regular (*top left*), that some are apparently chaotic (*top right, bottom left*), and that instability can arise at any timescale (*bottom right*). These long-term simulations show that regions exist in phase space in which this system can survive for at least 10^8 yr.

Several papers have suggested that secular resonance locking maintains stability in ESPSs with large eccentricities (Rivera & Lissauer 2000, 2001; Chiang et al. 2001). Specifically, they suggest that the orientation of the planets' ellipses should be aligned ($\Lambda \approx 0$). By examining Λ in stable, regular long-term simulations we can determine whether the longitudes of periastron remain locked. The probability distribution of Λ for these same four long-term simulations is presented in Figure 9. Λ is sampled once every 100 yr. The top left plot of Figure 9 is similar to that of an harmonic oscillator; this configuration is librating about $\Lambda = 0$ with an amplitude of 40°. The other plots are systems that are not librating, but instead show more random motion. From this figure we see that regular motion is correlated with libration about alignment, but chaotic and unstable motion generally shows chaotic Λ behavior.

3.2. *GJ 876*

Two planets orbit the $0.32 \pm 0.05\ M_\odot$ (Marcy et al. 2001a) M4 star GJ 876, also known as Gliese 876. This system is very similar to HD 82943, the major difference being that the planets lie closer to their primary. The semimajor axes of these two planets are 0.13 and 0.21 AU. Note that in this system planet c is the inner and less massive planet. A substantial amount of work has already been done on this system. The discovery

TABLE 2
Selected Simulations of HD 82943

Trial	$e_{b,0}$	$e_{c,0}$	R_0	Λ_0 (deg)	ϵ	Comments[a]
216	0.563	0.345	2.0108	42.2	2.6×10^{-7}	C, P (c, 299.9)
348	0.617	0.419	1.9656	13.6	1.5×10^{-8}	R
382	0.516	0.322	2.0303	32.4	9.2×10^{-9}	C
698	0.481	0.440	2.0948	68.4	1.3×10^{-10}	C, P (b, 7.5), E (b, 10.5)

[a] R = regular, C = chaotic, P = perturbed (planet, time [10^3 yr]), and E = ejected (planet, time [10^3 yr]).

paper (Marcy et al. 2001a) notes that stable configurations exist in the system. Lissauer & Rivera (2001) show that Keplerian fitting for this system is not precise enough to accurately determine the orbits. They suggest, through *N*-body fitting, that GJ 876 must actually lie in perfect resonance and that the orbital elements provided in the discovery paper (which are used here) suffer from a systematic error. Because P_1 is so short for this system (60 days), the evolution of the orbital elements has been observed and has corroborated this theory. Ji et al. (2002) also find that perfect resonance acts to stabilize this system. This section therefore serves as a check to this hypothesis.

We ran GJ 876 for 10^6 yr, but $\tau_{\mathrm{GJ\,876}}$ corresponds to only 47,000 yr. On 47,000 yr timescales, only 5.6% $\pm$ 2.8% of parameter space is stable. On 10^6 yr timescales, 2.4% of configurations survived, but only 1.7% were still unperturbed, and 5% failed to conserve energy. In unstable cases planet c, the inner and less massive, was ejected/perturbed nearly 96% of the time. Figure 10 shows the instability rate. GJ 876 shows the same trend as HD 82943; most unstable configurations break up in just a few hundred dynamical times. Again, the asymptotic nature of this plot implies that most unstable configurations have been identified. This system shows the same sort of trend in ϵ as HD 82943, which proves that our results our valid.

Unlike HD 82943, there are no obvious zones of stability. We see only isolated islands in the R-e_b stability map presented in Figure 11. We choose these parameters for our stability map because they were the strongest indicators of stability in HD 82943 and because of the suggestion that the system actually is in perfect resonance. Close to $R = 2.00$ we sampled two simulations near $R = 2.02$ and $e_b = 0.7$. Both of these were stable. However, with such poor statistics and at such a large (relative) distance from perfect resonance, we cannot comment on the likelihood that the system would be more stable in perfect resonance. We can, however, point out that there are isolated configurations that may hold stable orbits, and prolonged observations of this system should demonstrate whether it is indeed in perfect resonance. However, this lack of a large stable region strengthens the hypothesis that this system lies in perfect resonance.

This system does lies very close to $\Lambda = 0$. However, this proximity to alignment has no bearing on the stability of the system; in fact, it may actually diminish its chances of stability. In Figure 12 the probability of stability as a function of initial Λ is shown. Although the values for large Λ are poorly sampled, four data points at 100% stability does suggest that larger values of Λ may be more stable.

Similar dynamics are present in GJ 876 as in HD 82943. In Figure 13 and 14 we show two examples of stable and unstable configurations. The initial conditions for several simulations are listed in Table 4. In Figure 13 we plot the orbital evolution of simulation GJ 876−029, a stable, yet chaotic configuration. Although this system was stable for 47,000 yr, planet b was perturbed after 220,000 yr. This system, however, remained bound for 10^6 yr. The large eccentricity oscillations continue on to 10^6 yr, and planet c tends to remain in a retrograde orbit. After 10^6 yr $a_c = 0.0515$ AU, $0.06 \le e_c \le 0.85$, $i_c \approx 120°$, $a_b \approx 0.87$ AU, $e_b \approx 0.77$, and $i_b \le 5°$. The period of e_c oscillations remains at 3300 yr. The Λ evolution further belies the chaos in this system, since it tends toward antialignment but also circulates. As before, this distribution is over 10^6 yr, but since the system remains in approximately the same state from 25,000 yr to 10^6 yr, this plot is a fair representation of the motion during the first $\tau_{\mathrm{GJ\,876}}$.

In Figure 14 the evolution of a system which perturbs the outer planet in just 9000 yr is shown. The system ejects planet b in 152,000 yr. Before reaching $\tau_{\mathrm{GJ\,876}}$ this system experiences some remarkable evolution in *a*, *e*, and *i*. Note, too, that Λ very quickly moved to an antialigned configuration.

Long-term simulations for this system were integrated for 27.5 million years. A complete summary of the long-term simulations for this system is presented in Table 5. Figure 15 plots the eccentricity evolution of four simulations. Some

TABLE 3
Results of Long-Term (10^8 yr) Simulations of HD 82943

Trial	$e_{b,0}$	$e_{c,0}$	R_0	Λ_0 (deg)	ϵ	Result[a]
000	0.561	0.395	2.0269	26.5	5.2×10^{-8}	C
021	0.571	0.333	2.0615	39.0	1.0×10^{-8}	C
032	0.414	0.556	2.0556	33.3	4.95	ϵ(2.4), E (b, 2.4)
035	0.511	0.236	2.0322	6.7	6.8×10^{-9}	R
036	0.534	0.197	2.0080	29.5	6.1×10^{-9}	R
040	0.600	0.393	2.0766	52.8	0.22	ϵ(1.005), E (c, 1.14)
043	0.542	0.386	2.0223	24.8	2.4×10^{-8}	C
057	0.549	0.348	2.0382	27.0	1.1×10^{-8}	C
073	0.468	0.265	2.0626	56.8	6.3×10^{-8}	R

[a] R = regular, C = chaotic, ϵ = energy conservation failed (time [10^6 yr]), and E = ejection (planet, time [10^6 yr]).

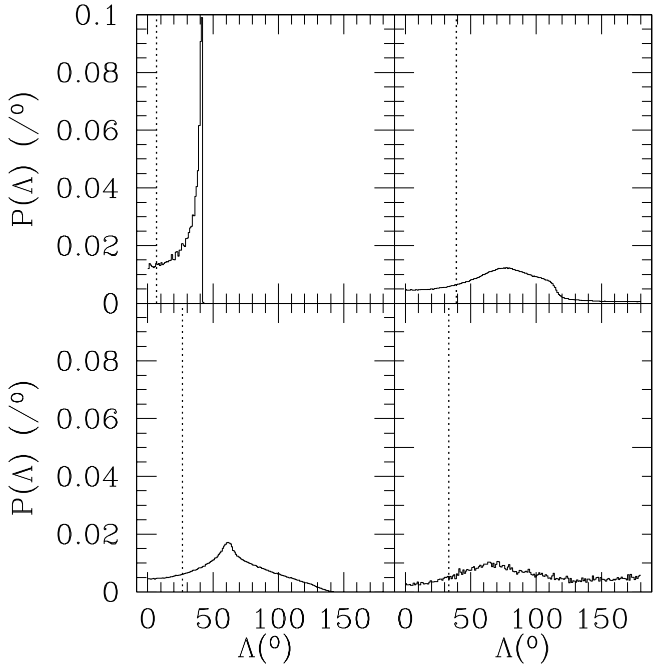

FIG. 9.—Distribution function of Λ (sampled every 100 yr) for four stable cases of HD 82943. These four systems are the same as in Fig. 8. The top left plots a system librating about $\Lambda = 0$. The other plots show that chaotic and unstable motion is usually associated with a circulating Λ.

systems appear regular throughout (*top left*). Some configurations are chaotic for the duration of the simulation (*top right, bottom left*), and others may eject a planet after an arbitrarily long period of time (*bottom right*).

Figure 16 shows the distribution function of Λ for the same four systems. The regular system (*top left*) shows a configuration that usually librates with an amplitude of 80°, but with occasional circulation. The two chaotic examples (*top right, bottom left*) have flat distribution functions. Not surprisingly, the unstable trial shows a very peculiar distribution function.

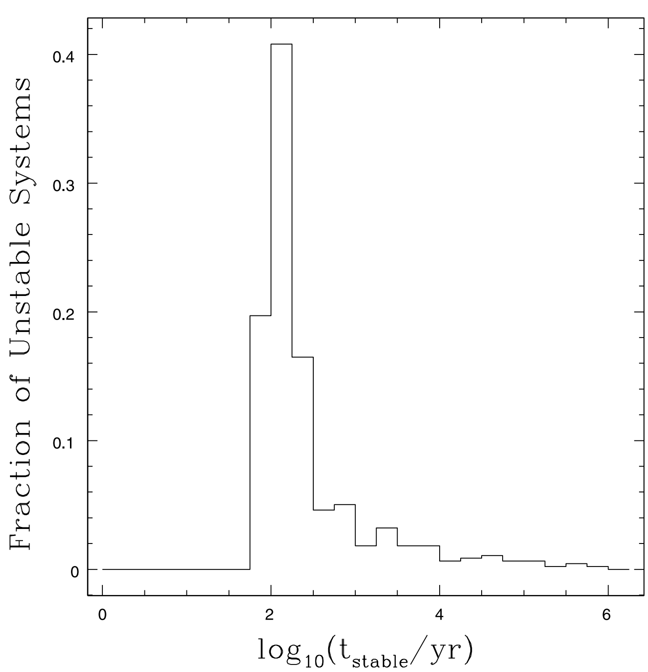

FIG. 10.—Ejection rate for GJ 876. In this system unstable configurations are usually ejected within 100 yr. The rate asymptotically falls to zero by 10^5 yr.

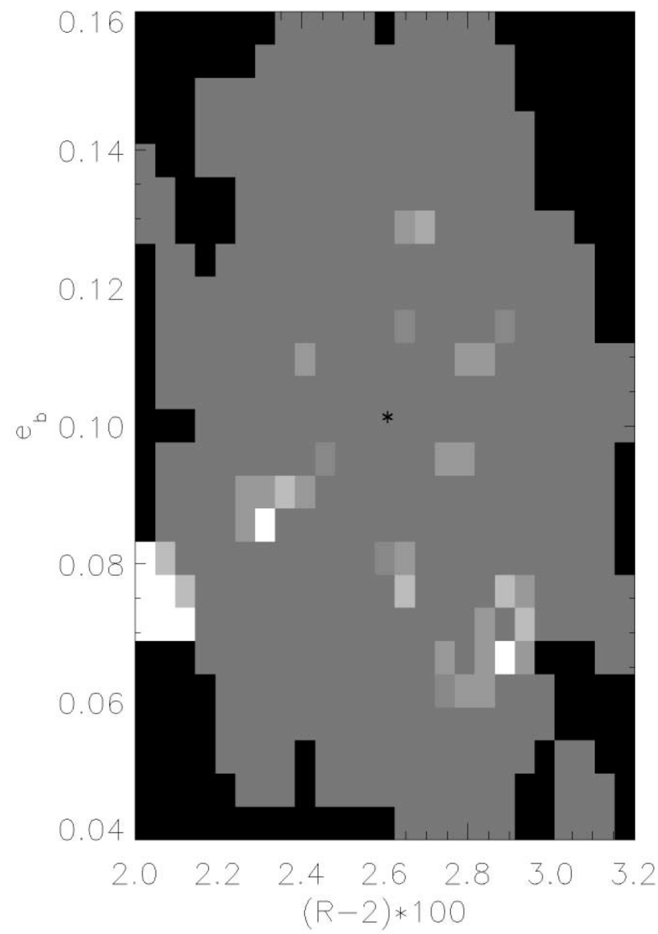

FIG. 11.—R-e_b stability map for GJ 876. The asterisk marks the best fit to the system as of 2002 August 7, and the values for stability are more accurate closer to the asterisk. In this system, as in HD 82943, the two relevant orbital elements are e_1 and R. There are no contiguous regions of stability, only small isolated pockets that may hold stable zones.

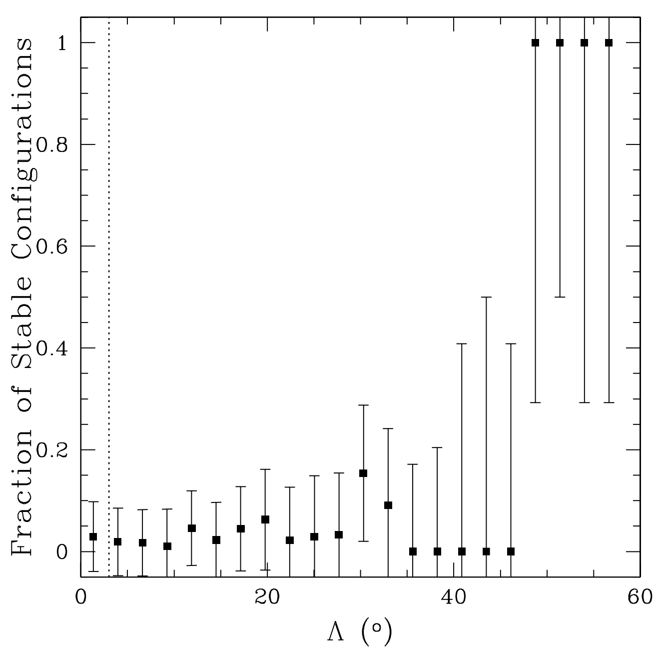

FIG. 12.—Dependence of stability on initial Λ. The data above 50° are poorly sampled, but with such a large difference between their values and the mean of 5.7%, they do suggest that stability may be improved at $\Lambda \gtrsim 50°$.

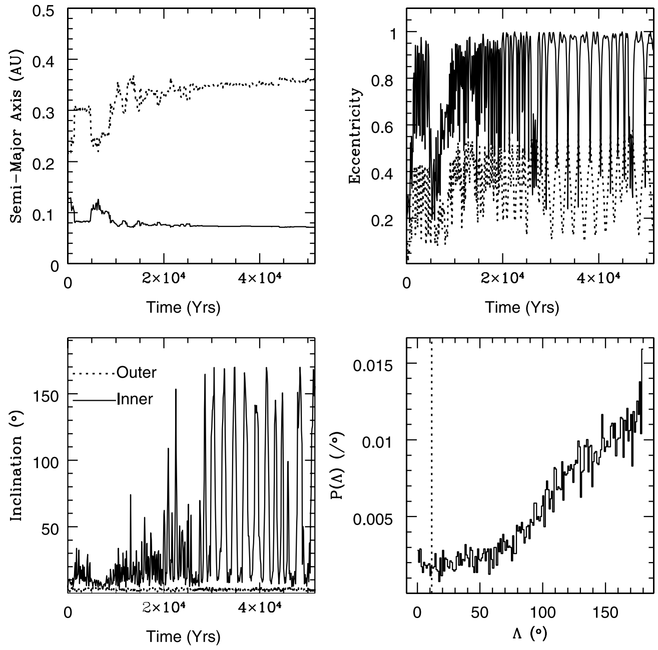

FIG. 13.—Orbital evolution of GJ 876−029, a chaotic stable configuration of GJ 876. *Top left:* Although the semimajor axes vary, they do not change by a factor of 2 until 220,000 yr = $4.7\tau_{\rm GJ\,876}$. *Top right:* The remarkable eccentricity evolution of this system. These oscillations persist for 10^6 yr. *Bottom left:* The inclination of planet b varies a small amount, generally staying below 5°. Planet c experiences wild fluctuations; however it does eventually settle to 120°. *Bottom right:* This curious Λ distribution function suggests that Λ prefers antialignment. This implies that a protection mechanism is keeping the system from breaking apart despite the extremely large values of $e_{\rm b}$.

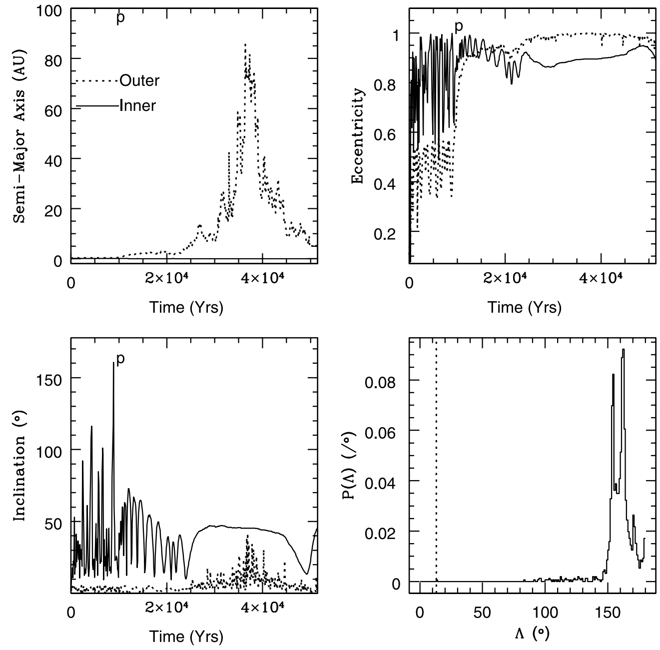

FIG. 14.—Orbital evolution of GJ 876−858, the perturbation of GJ 876b. Planet b was eventually ejected after 152,000 yr. *Top left:* The semimajor axes evolve quiescently for 9000 yr, until a close approach increases $a_{\rm b}$, marked by the *p*. Although $a_{\rm b}$ returns to its initial value by $\tau_{\rm GJ\,876}$, just prior to ejection $a_{\rm b}$ reached 750 AU. *Top right:* The eccentricities immediately jump to very large values. Values of $e_{\rm c}$ vary wildly between 0.6 and 0.99. After b is kicked out to large *a*, the oscillations become much smaller. For nearly 10,000 yr $e_{\rm b}$ remains above 0.98, but it does not reach unity until 152,000 yr. *Bottom left:* As with eccentricity, the inclination of c jumps wildly for 9000 yr, even reaching 162° just prior to perturbation. *Bottom right:* As with the *e* and *i*, Λ immediately moves from its starting position. However, Λ remains very close to antialignment for the duration of the simulation.

As in HD 82943, we see that regular systems tend to librate and chaotic configurations circulate.

Although the evidence is compelling that GJ 876 does in fact lie in perfect resonance, our work demonstrates that stable, regular systems do exist close to the observed Keplerian fit. More observations of this system will demonstrate whether the system is in perfect resonance. This work clearly demonstrates that stable regions do exist for a system like GJ 876 just beyond perfect resonance. Should this system lie in perfect resonance, then this work shows that unstable regions lie very close to its configuration.

New astrometric data has confirmed the mass of the outer planet in this system (Benedict et al. 2002). This is therefore the only ESPS with a known mass. The plane of b's orbit is inclined by 6° to the line of sight. Benedict et al. confirm the mass and semimajor axis of this planet to be statistically identical to those presented in Table 1. However, for this paper, the lack of data for planet c precludes any new insights into the dynamics of the system. At best, if the system is approximately coplanar, then the variations used here are indeed representative of the true system, and our results are more robust.

4. INTERACTING SYSTEMS

Four known systems meet the interacting system criterion: υ And (Butler et al. 1999), 47 UMa (Fischer et al. 2002), the SS,[3] and HD 12661 (Fischer et al. 2003). In this paper we will limit ourselves to the first three. The number, placement, and sizes of the planets in each system are quite different, but all have at least two planets that lie in between the 2:1 and 10:1 resonances. υ And was the first known ESPS and was the subject of Paper I. The experiment in Paper I is the procedure for this paper, and the simulations have been performed again. 47 UMa was announced in 2001 and, at first glance, appears more like the SS than υ And. Performing this experiment on the SS is problematic. The errors in the orbital elements of the SS are drastically smaller than for the ESPSs, and therefore fitting the SS into the procedure requires inflating the SS orbital element errors to values comparable to those of the ESPSs. Essentially we are asking what would we observe if we took radial velocity measurements of our Sun. We will compare the ESPSs to both the gas giant system (§ 4.3) and the Jupiter-Saturn system (§ 4.4). These three coupled systems' orbital elements are summarized in Table 6. Interacting systems show broad regions of stability that are correlated with eccentricity.

4.1. υ *Andromedae*

The υ And system is a combination of a separated system and an interacting system. Three planets orbit the $1.02 \pm 0.03\ M_\odot$ (Gonzalez & Laws 2000) F8 star υ And. The inner planet, b, orbits at 0.04 AU. The other planets, c and d, orbit at larger distances (0.8 and 2.5 AU, respectively) but are significantly more eccentric. The outer planet is the most massive; therefore $\tau_{\upsilon\,\rm And}$ corresponds to 10^6 yr.

The υ And system was the subject of Paper I and has been the focus of intense research since its discovery. The apparent alignment of the apses of planets c and d has sparked the most interest, with several groups claiming that the system must be secularly locked, or at least librate about $\Lambda = 0$ (Rivera & Lissauer 2000; Lissauer & Rivera & 2001; Chiang & Murray

[3] See http://ssd.jpl.nasa.gov/elem_planets.html.

TABLE 4
Selected Simulations of GJ 876

Trial	$e_{c,0}$	$e_{b,0}$	R_0	Λ_0 (deg)	ϵ	Comments[a]
029	0.177	0.073	2.0241	11.6	4.6×10^{-5}	C
563	0.239	0.122	2.0247	3.65	2.2×10^{-8}	C, P (b, 5.1), E (b, 5.3)
858	0.338	0.107	2.0255	13.1	6.2×10^{-6}	C, P (c, 14.9), E (c, 151.9)
904	0.351	0.072	2.0303	51.0	2.7×10^{-9}	R?

[a] R = regular, C = chaotic, P = perturbed (planet, time [10^3 yr]), and E = ejected (planet, time [10^3 yr]).

2002), while others suggest that this alignment may be a chance occurrence (Paper I; Stepinski et al. 2000). However, these groups and others (Laughlin & Adams 1999) all agree that this system, as presented, can be stable for at least 10^8 yr.

On a 10^6 yr timescale, 86.1% $\pm$ 3.3% of simulations survived, and 0.4% failed to conserve energy. This value is less than 1 σ from the value published in Paper I, 84.0% $\pm$ 3.4%. Figure 17 shows the perturbation rate as a function of time. Once again we see that most unstable configurations eject a planet immediately, and the rate falls to 4% by 10^6 yr. The fact that ejections occur right up to 10^6 yr implies that we have not detected all unstable situations and that the stability map for this system contains more unstable configurations, and hence the plateau is smaller and/or the edge is steeper after 10^9 yr.

There is one notable difference between the results of Paper I and those reported here: the frequency of ejections of each planet is different. In Paper I planet b was ejected 10% of the time, c, 60%, and d, 30%. The SWIFT runs ejected planet b 39% of the time, c, 54%, and d, 7%. Figure 18 plots the survival probability in this system as a function of energy conservation. Stability peaks at $\epsilon = 10^{-8}$ but quickly drops. Although this plot is qualitatively different from Figure 2, we again note that this implies that the simulations are valid. This plot is typical for the interacting systems, confirming our hypothesis that we need only maintain $\epsilon < 10^{-4}$ for the duration of every simulation.

In Paper I a stability map in e_c and e_d was presented in Table 2. This table showed that e_d and, to a lesser degree, e_c determined the stability of the system. In Figure 19 the υ And stability map is presented, which is nearly an exact match to that in Paper I. However, the best fit to the system[4] has changed since then and the system has moved away from the edge slightly. From Figure 19, it is clear that υ And lies close to instability but not right on the edge. The edge of stability in υ And, however, is fundamentally different from in resonant systems. In this interacting system, a large region of phase space is fully stable (the ''plateau''), but there is a sharp boundary in eccentricity space (the ''edge''), beyond which the system quickly moves into a fully unstable region (the ''abyss''). Although it appears that both morphologies are on the edge of stability, they are different types of edges.

As previously mentioned, there are some unusual features of this system; the lines of node are nearly aligned, and the system lies close to the 11:2 mean motion resonance. This is a weak perturbation, but between these two massive planets, this may be important. However, a quick inspection of plots of stability versus Λ (Fig. 20) and R, not presented, shows that there is no statistically significant affect caused by these two (potential) resonances. We do note that our integration time may not be long enough to detect the importance of the 11:2 resonance.

As has been shown in other papers, this system exhibits both apparently regular and chaotic motion. In Figures 21 and 22 we present examples of orbital evolution of this system. Table 7 lists the initial conditions and results of several configurations. In Figure 21 the orbital evolution of a regular, stable configuration is plotted. However, this plot actually demonstrates the breakdown of our model. Planet b's eccentricity oscillates with an amplitude of 0.3 and a period of 120,000 yr. Unfortunately, υ And b is tidally locked by its parent star with a period of 0.011 yr. The timescale for tidal circularization is 8×10^7 yr (Trilling 2000). We address this potential inconsistency in § 7. Λ for this system librates with an amplitude of 50°, an indicator of regular motion.

In Figure 22 we show the orbital evolution of a system that perturbs planet d but ejects planet c. The behavior of the

[4] See http://exoplanets.org/upsandb.html.

TABLE 5
Results of Long-Term (27.5×10^6 yr) Simulations of GJ 876

Trial	$e_{c,0}$	$e_{b,0}$	R_0	Λ_0 (deg)	ϵ	Result[a]
290	0.0884	0.248	2.02353	45.3	2.4×10^{-9}	C
300	0.108	0.161	2.02641	15.2	0.5	ϵ(4.06), E (b, 4.08)
362	0.124	0.366	2.02624	29.3	2.6×10^{-8}	R
404	0.121	0.246	2.02548	46.43	0.6	ϵ(17.6), C
609	0.0875	0.241	2.02342	53.5	2.5×10^{-9}	R
655	0.110	0.256	2.02601	13.9	0.19	ϵ(11.2), P (b, 24.0)
661	0.105	0.208	2.02778	33.1	0.18	ϵ(2.4), E (c, 2.4)
739	0.107	0.273	2.02726	31.2	0.02	ϵ(1.4), E (b, 1.4)
895	0.0816	0.228	2.02242	19.4	2.3×10^{-8}	C
948	0.0628	0.204	2.02803	4.80	4.1×10^{-4}	ϵ(0.25), C

[a] R = regular, C = chaotic, ϵ = energy conservation failed (time [10^6 yr]), P = perturbed (planet, time [10^6 yr]), and E = ejected (planet, [10^6 yr]).

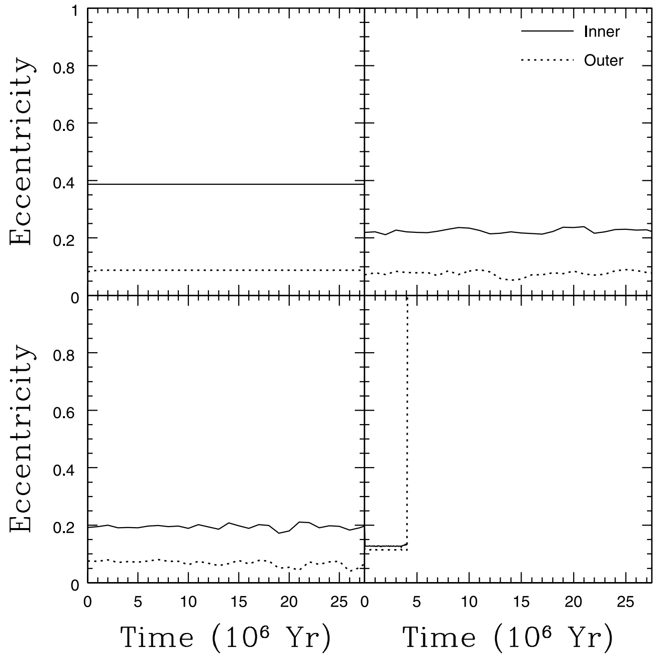

FIG. 15.—Eccentricity of four long-term simulations of GJ 876. *Top left:* Evolution of GJ 876−362, an apparently regular configuration. *Top right:* Evolution of GJ 876−290, a chaotic, yet stable configuration. *Bottom left:* Evolution of GJ 876−895, a chaotic, stable configuration. *Bottom right:* Evolution of GJ 876−300 which ejects planet b after four million years.

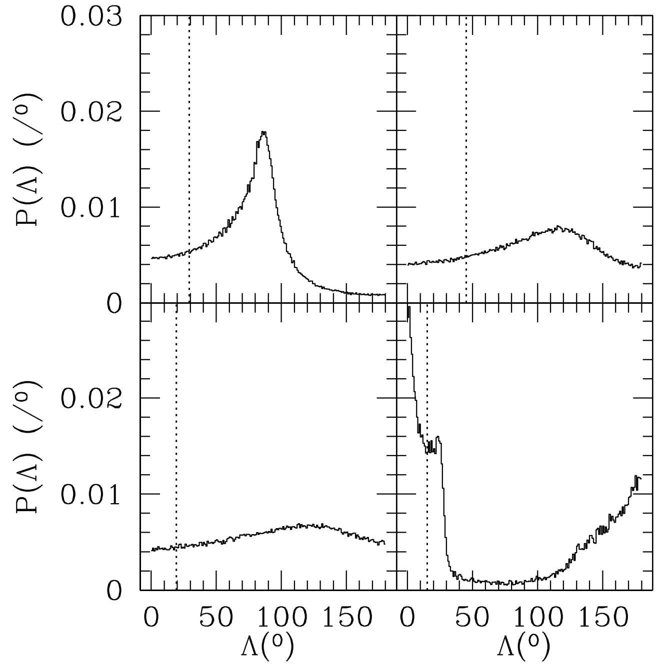

FIG. 16.—Λ evolution of the same four simulations in Fig. 19. Chaotic systems (*top right, bottom left*) show no signs of libration, while regular systems (*top left*) are librating, but with occasional circulation. The unstable example (*bottom right*) shows a very strange distribution, which only demonstrates the chaos of this system.

ejecting planet reaching very large semimajor axis distances and subsequently returning, only to be ejected, was also seen in GJ 876 (see Fig. 14). Note, too, that the peak in e_b corresponds with the peak in i_b.

Long-term simulations run for 100 million years. Figure 23 is the eccentricity evolution of four simulations. In one case (Fig. 23, *bottom right*) the inner planet is ejected after 55 million years. The top left panel shows a system undergoing chaotic evolution. The other two panels show regular motion.

Figure 24 shows the Λ distribution of these configurations. Several different modes of stability exist for the apses in this system. The panels in Figure 24 correspond to those in Fig. 23, and therefore the top left is the regular case. The apparently chaotic systems (*top right, bottom left*) show the Λ distribution signature of chaos, as does the example which ejects planet b (*bottom right*). In Table 8 we present a summary of all long-term simulations for υ And.

4.2. *47 UMa*

The 47 UMa system consists of a $1.03 \pm 0.03\ M_\odot$ (Gonzalez 1998) star and two interacting companions: b and c, at 2.09 and 3.73 AU, respectively. The initial eccentricities in this system are substantially lower than υ And at 0.06 and 0.1,[5] respectively. More recent measurements place e_c much closer to 0. However, "$e_c = 0.3$ provides almost as good a fit to the radial velocity data as does $e_c = 0\farcs005$" (Laughlin et al. 2002). Should $e_c \leq 0.1$ then, of all the systems examined in this paper, 47 UMa most closely resembles our own. Planet b is the larger planet and hence determines $\tau_{47\ \mathrm{UMa}} = 840,000$ yr.

Overall, $80.3\% \pm 4.7\%$ of simulations were stable to $\tau_{47\ \mathrm{UMa}}$. This is less than a 2 σ difference from υ And. In unstable configurations planet c, the less massive planet, was ejected every time. This is similar to υ And, in which the most massive planet perturbed the smaller planets. The instability rate as a function of time is presented in Figure 25. The rate for 47 UMa is similar to the other systems in that most unstable configurations perturb a planet past stability on relatively short timescales, but with a tail to longer times. The rate does not reach zero, however, and suggests that more unstable configurations exist.

The 47 UMa stability map is presented in Figure 26. The overall structure of stability in eccentricity space is qualitatively the same as in υ And, with one major exception: stability is correlated with e_2 (e_c), not e_1 (e_b). The errors for e_c are substantial. The main difference between 47 UMa and υ And is that the more massive companion is the interior planet. This configuration makes it more difficult for the exterior planet to perturb the interior planet, which is more tightly bound to the parent star.

This stability map is in good agreement with other work done on this system. Using MEGNO, Goździewski (2002) determined the maximum value for e_c to be approximately 0.15. A stability analysis in Laughlin et al. (2002) also shows a similar dependence on e_c. For nearly coplanar systems, such as those presented here, they determined the maximum value for e_c to be less than 0.2. Although the exact maximum value for e_c is different for all three studies, it is clear that the value of e_c determines stability for 47 UMa.

When comparing Figure 26 with Figure 19, we see that the edge in the υ And system is much cleaner than in 47 UMa. One possible reason for this is the system's proximity to the 5:2 mean motion resonance. To examine this possibility, in Figure 27 we plot stability as a function of R in this system. Although there appears to be some increase in stability beyond 5:2, and a decrease inside 5:2, the errors are too large to confirm whether this is a real effect.

In Figure 28 and 29 we present two possible orbital evolutions for 47 UMa. Some sample simulations from the suite of

[5] See http://exoplanets.org.

TABLE 6

Initial Conditions for Interacting Systems

System	Planet	Mass (M_J)	Period (day)	Eccentricity	Longitude of Periastron (deg)	Time of Periastron (JD)
SS	Jupiter	1.000	4331.6 ± 43.3	0.0484 ± 0.1	14.8 ± 90.0	2449896.3 ± 25.0
	Saturn	0.297	10759.7 ± 107.8	0.0542 ± 0.1	92.4 ± 90.0	2450411.1 ± 25.0
	Uranus	0.0459	30704.9 ± 307.0	0.0472 ± 0.1	171.0 ± 90.0	2447230.0 ± 25.0
	Neptune	0.0541	60197.2 ± 602.0	0.0086 ± 0.1	45.0 ± 90.0	2442071.3 ± 25.0
υ And	b	0.69	4.61706 ± 0.0003	0.015 ± 0.015	32.0 ± 243.0	2459991.588 ± 3.1
	c	1.96	241.1 ± 1.1	0.25 ± 0.11	251.0 ± 33.0	2450160.1 ± 20.8
	d	3.98	1309.0 ± 30.0	0.34 ± 0.11	255.0 ± 17.0	2450044.0 ± 40.5
47 UMa	b	2.54	1089.0 ± 3.0	0.06 ± 0.014	172.0 ± 15.0	2453622.0 ± 34.0
	c	0.76	2594.0 ± 90.0	0.1 ± 0.1	127.0 ± 56.0	2451363.5 ± 493.0

1000 are listed in Table 9. First, in Figure 28, is a stable regular configuration. Over 50% of all configurations for this system are regular. In this case the eccentricities, and inclinations show very small oscillations (10%) and Λ librates with an amplitude of 45°.

In Figure 29 we present an example of the ejection of planet c. This system appears to evolve regularly for 10,000 yr, then experiences 25,000 yr of chaotic evolution, culminating in the ejection of the outer planet. For this configuration Λ circulates during the first 30,000 yr, both regular and chaotic epochs, but with different angular velocities in each stage. During the final 10,000 yr, however, when e_c becomes very large, Λ becomes locked at 155°.

Long-term simulations of 47 UMa were integrated for 10^9 yr. Table 10 is a summary of all long-term simulations for 47 UMa. Figure 30 shows the eccentricity evolution of four systems. The top right panel of this figure is fascinating. The system is very chaotic for the first 350 million years, then enters a short (~20 million years) period of quiescence, only to return again to a similar chaotic state. The other configurations all appear regular. Figure 31 plots the Λ evolution. In 47 UMa no secular resonance locking occurs. However, these plots confirm the results of Laughlin et al. (2002). They show that for low values of e_c (<0.1) the system should librate in an aligned configuration, but above 0.1 the system should be antialigned. The chaotic case, as expected, has a flat distribution function.

4.3. *Gas Giants*

Perhaps the most interesting aspect of the new ESPSs is their comparison to the SS. The procedure outlined in § 2 permits a comparison of the ESPSs and the SS. We must first, however, determine how to vary the initial conditions of the gas giants. As can be seen in Table 6, the "error" associated with each planet is arbitrary. We have given a spread in initial conditions that is roughly similar to the percent error as listed in the ESPSs. For example, the periods are allowed to vary by approximately 10%, but the eccentricities have a standard deviation of 0.1 for all planets. This procedure will allow us to create a stability map for the SS but will make a comparison of the probabilities of survival less meaningful.

The outer SS consists of four gas giants located between 5.2 and 40 AU. The gas giants are on much more circular orbits

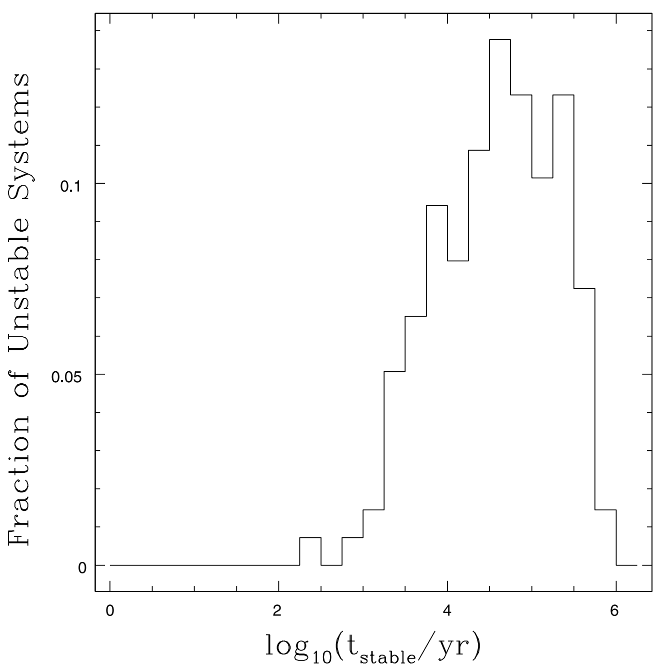

Fig. 17.—Ejection rate of unstable configurations in υ And. Configurations may eject planets right up to 10^6 yr. It is therefore unclear how many more configurations might become unstable.

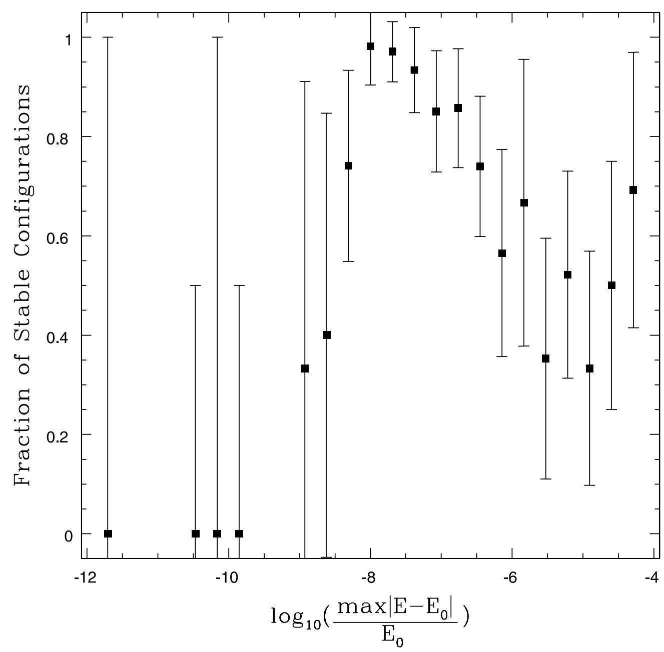

Fig. 18.—Survival probability as a function of energy conservation in υ And. The instability at low ϵ implies that the results for υ And are robust.

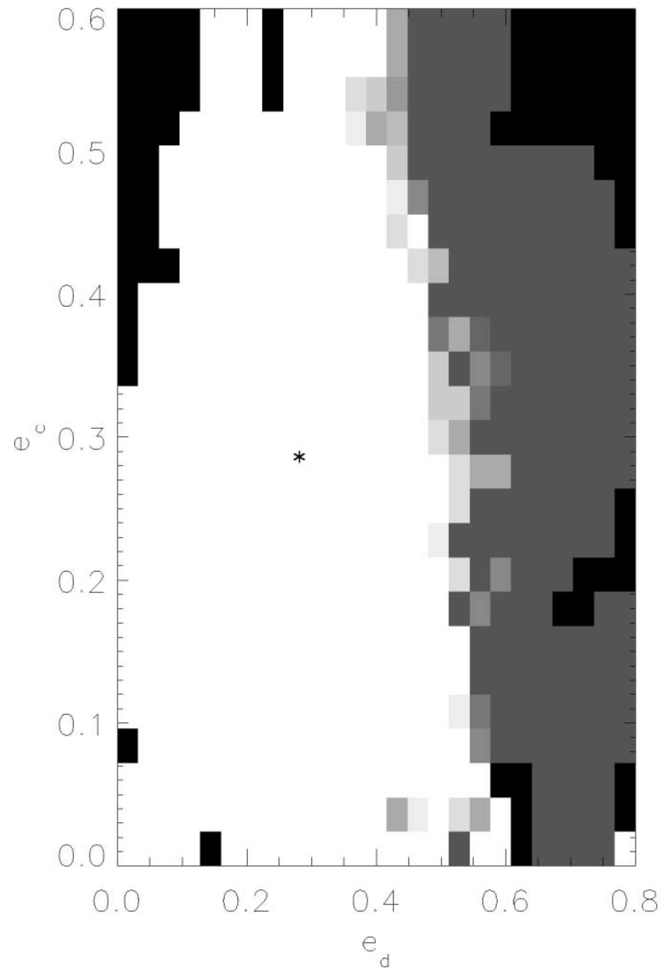

FIG. 19.—Stability map for υ And. Stability in this system depends on e_d and, to a smaller degree, on e_c. As in resonant system stability maps, precision is correlated with distance from the asterisk, which marks the best fit to the system as of 2002 September 24. υ And lies near the edge of stability.

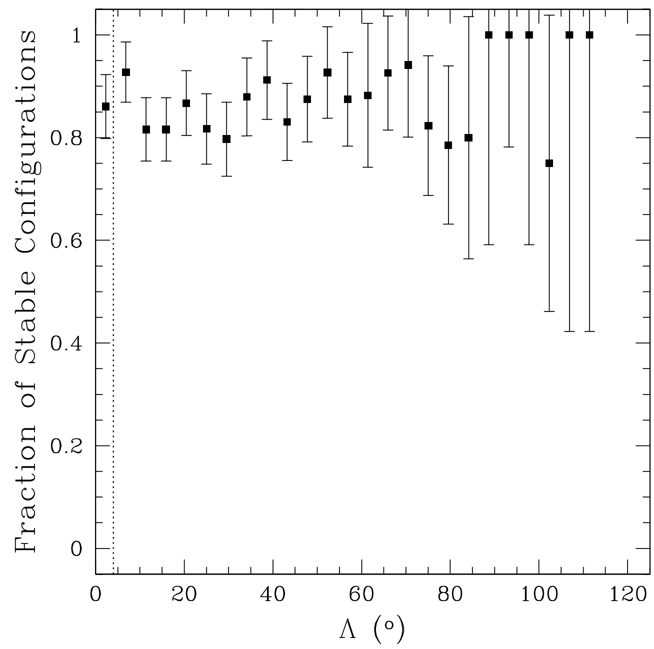

FIG. 20.—Stability as a function of Λ in υ And. Although the best fit to the system places it very close to alignment, marked by the dashed vertical line, there is no significant trend with Λ.

than the ESPS planets (Saturn has the largest eccentricity at just over 0.05). Because of the large semimajor axes, τ_{SS} corresponds to 3.32×10^6 yr. Compared to known ESPSs, the gas giants are relatively low-mass planets. In fact Uranus and Neptune could not be detected via the Doppler method at the precision level currently achieved (see § 4.4).

Chaos in the SS is well documented (e.g., Sussman & Wisdom 1988, 1992; Varadi et al. 1999; Lecar et al. 2001). In fact, Varadi et al. (1999) show that the Jupiter-Saturn system lies very near chaotic regions. They vary the semimajor axes of these two planets slightly (less than 1%) and find that this is enough to identify broad chaotic regions. Below we show that by enlarging this variation, the system moves into total instability; ejections are inevitable.

For the gas giants 85.3% ± 4.3% of the trials were unperturbed for 3.3×10^6 yr. Paper I integrated 32 gas giant configurations, and 81% of these survived. As in § 4.1, we again recover the results of Paper I. In this system Jupiter was never ejected; it always removed the other planets from the system. Saturn was ejected in 14% of the simulations, Uranus (the least massive) in 62%, and Neptune in 24%. In the SS therefore, the ejection rate is tightly coupled to mass, as was observed in the other ESPSs. It therefore seems that the SS behaves like other interacting systems.

Figure 32 shows the instability rate. Most configurations survive for 10^5 yr. Once again it appears the perturbation rate does not fall to zero, and we note that this means that we have not found all the unstable systems. The last bin in this plot contains only 20,000 yr worth of data. It is therefore unclear whether the ejection rate might still be rising with larger time. Should that be the case, our choice for τ_{SS} is too small, suggesting that we have not identified all unstable configurations. Figure 33 is the stability map for the gas giants. The gas giants show a plateau as in 47 UMa and in υ And; however, the edge is much less dramatic. The actual values for our gas giants show that our system lies quite far from the stability edge. We also note that the stability plateau shows many depressions and that the abyss contains many spires. This apparent difference between the SS and other interacting systems may result from not identifying all unstable configurations. Perhaps longer integrations would sharpen the edge and broaden the instability abyss. Dynamically, the major difference between the SS and other interacting systems is that the SS has a much broader range of orbital times. Jupiter orbits 13 times more quickly that Neptune. Perhaps instability is more relevant on the timescale based on the orbit of Neptune (see § 6). However, these features may also arise from the system's proximity to the 5 : 2 resonance, the so-called great inequality. We address this possibility in § 4.4.

Several example simulations are shown in Figures 34–36. The initial conditions and outcomes of these simulations are shown in Table 11. The best fit to e_J, e_S, and R is simulation SS-183. The orbital evolution of this system is shown in Figure 34. Note, however, that Λ_0 differs substantially from its standard value of 68°.5. This difference is responsible for the chaotic evolution of e_J and e_S. Curiously, though, the evolution of e_U and e_N are regular. Unlike the eccentricities, all the inclinations evolve regularly. The nodes of Uranus and Neptune librate about antialignment, but with occasional circulation. Note that in e and i Uranus oscillates from two modes,

TABLE 7

Selected Simulations of υ And

Trial	$e_{c,0}$	$e_{d,0}$	R_0	Λ_0 (deg)	Comments[a]
000	0.276	0.486	5.583	38.3	C, P (c, 218), E (b, 218)
014	0.177	0.470	5.509	20.2	C, P (d, 219), E (d, 219)
020	0.299	0.532	5.207	21.7	C, P (d, 10.1), E (c, 31.3)
076	0.394	0.375	5.566	11.1	R
236	0.168	0.428	5.386	81.0	C

[a] R = regular, C = chaotic, P = perturbed (planet, time [10^3 yr]), and E = ejected (planet, time [10^3 yr]).

whereas Neptune experiences three modes. We also note than an examination of the Fourier power spectrum of Poincaré's h and k variables shows that Jupiter and Saturn's motion is the result of numerous short, broad peaks. Their motions are therefore best described as chaotic.

In Figure 35 a fully chaotic, yet stablen configuration is shown. The semimajor axes show obvious signs of encounters but never change by more than 20%. The eccentricities are very chaotic, but rarely reach 0.3. The inclinations, too, are extremely chaotic, but never surpass 12°. The double-peaked Λ distribution function is another clear indicator of chaos.

The ejection of Uranus is shown in Figure 36. The semimajor axes of Jupiter and Saturn remain nearly constant throughout the simulation, but Neptune and Uranus are clearly interacting. The eccentricities are chaotic but remain near the starting values, except for Uranus, which steadily increases until it is ejected after 2×10^6 yr. The inclinations are also chaotic. Jupiter and Saturn appear quasi-periodic, while Neptune and Uranus are fully chaotic. The longitudes of periastron tend to remain near alignment, but the three peaks clearly belie the chaos in the system.

We ran no long-term simulations on the SS. The orbital elements for the SS are well determined, and many long-term simulations have already been performed on this system (see Duncan & Quinn 1993; Lecar et al. 2001).

4.4. *Jupiter and Saturn*

As mentioned above, Uranus and Neptune do not provide enough reflex velocity, K, motion in the Sun to be observable by current technology ($K \sim 3$ m s^{-1}). Should any planet of Uranus or Neptune mass exist in the observed ESPSs they would not be detected. Therefore we followed the same procedure with just Jupiter and Saturn. This suite of simulations can also provide clues as to how other ESPSs will behave if they have additional, distant companions.

Not surprisingly, this three-body system is more stable than the five-body system, as 96.3% ± 2.4% of the trials remained stable. In this system Jupiter was ejected 6.9% of the time, and Saturn 93.1%. It seems as though instability is being passed through Saturn and into the smaller planets. We can therefore apply this result to the other ESPSs. This Jupiter-Saturn system is analogous to the 47 UMa system. The mass ratio of the planets are about the same, as is R. The only substantial difference is that the masses are higher and the orbits closer in 47 UMa. However, our simulations of 47 UMa used $e_c = 0.1$. This is about twice as high as e_S. This decrease in eccentricity is clearly important as the Jupiter-Saturn system is substantially more stable than 47 UMa. This again demonstrates that the eccentricities of the planets are key in determining stability.

Figure 37 is the stability map for the Jupiter-Saturn system. This plot is similar to Figure 33. There is a boundary at approximately the same location in eccentricity space; however, the drop is not so sharp or so deep as in the gas giant system. Further, an additional plateau rises at larger eccentricities. This last phenomenon is not observed in any other system in this paper.

As mentioned in § 4.3, stability might be correlated with the 5:2 resonance. Figure 38 shows stability as a function of R for the SS. There is a hint that as the system moves out of this third-order resonance, stability increases, but the errors on these distant configurations are too large to confirm this possibility. In 47 UMa $R = 2.38$, while in the SS, $R = 2.48$. Although there are no statistically meaningful points in Figures 27 and 38, the same trend appears in both, namely, that interior to 5:2 instability is more prevalent. As has been shown throughout this paper, the eccentricities determine the overall stability, and the statistics are too poor to claim any trend with R in either system; note that no point differs by more than 1 σ from the mean instability rate.

Comparing the gas giants with Jupiter-Saturn provides us with an excellent opportunity to explore completeness. As mentioned above, the Jupiter-Saturn system is similar to 47 UMa, yet the stability maps are quite different. The Jupiter-Saturn system is the only system examined with no instability abyss, and it is the only system we know to be incomplete.

5. SEPARATED SYSTEMS

By the end of 2002 three separated systems had been announced: HD 83443,[6] HD 168443 (Marcy et al. 2001b), and HD 74156.[7] The values and errors for these systems are reproduced in Table 12. HD 83443 consists of two Saturn-mass planets in very tight orbits. HD 168443 consists of two very large companions ($m_1 \geq 17M_J$, $m_2 \geq 7.5M_J$). In fact, planet c should be considered a brown dwarf, and if the system is more inclined than 35°, planet b would also be a brown dwarf. For this system $R = 30.5$. HD 74156 contains two bodies of slightly more than a Jupiter mass, with $R = 44.6$. We examined only HD 168443 and HD 83443. Evidence is mounting that HD 83443 is not a multiple system (Butler et al. 2002); therefore we stopped the simulations on this system after 847 trials had been completed. For HD 168443 and HD 83443, all simulations survived to τ. HD 74156 has a larger R and smaller masses than HD 168443. It therefore seems highly doubtful that any simulation of HD 74156 would produce an unstable configuration.

Although all simulations were stable, the dynamics of HD 168443 are still interesting. The eccentricities and inclinations of this system show a weak planet-planet interaction. Although no evidence of chaos is evident, the planets apparently are close enough that they feel each other. This system may be fully stable, but it appears to lie close to the

[6] See http://obswww.unige.ch/~udry/planet/hd83443_syst.html.

[7] See http://obswww.unige.ch/~udry/planet/hd74156.html.

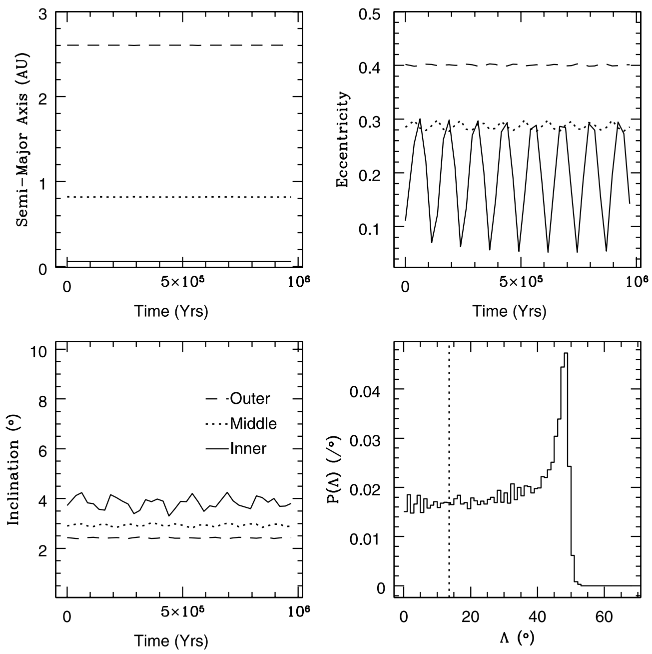

FIG. 21.—Orbital evolution of υ And-076, a stable, regular configuration, smoothed on 25,000 yr intervals. *Top left:* The semimajor axes show no evidence of perturbations. *Top right:* The eccentricities experience simple sinusoidal variations. The period of planet b oscillations is 100,000 yr, while c and d oscillate on a 7000 yr period. The large amplitude of e_b is most likely unphysical due to tidal locking with the parent star. The apparently irregular behavior of e_b is an artifact of its long cycle. *Bottom left:* The inclinations are also regular, although planet b's inclination is affected by both planets on its 20,000 yr period. Planets c and d oscillate in inclination on a 4000 yr period. As in eccentricity, the slightly chaotic appearance of i_b is an artifact of the sampling time convolved with the physical period. *Bottom right:* The Λ distribution librates with an amplitude of 50°.

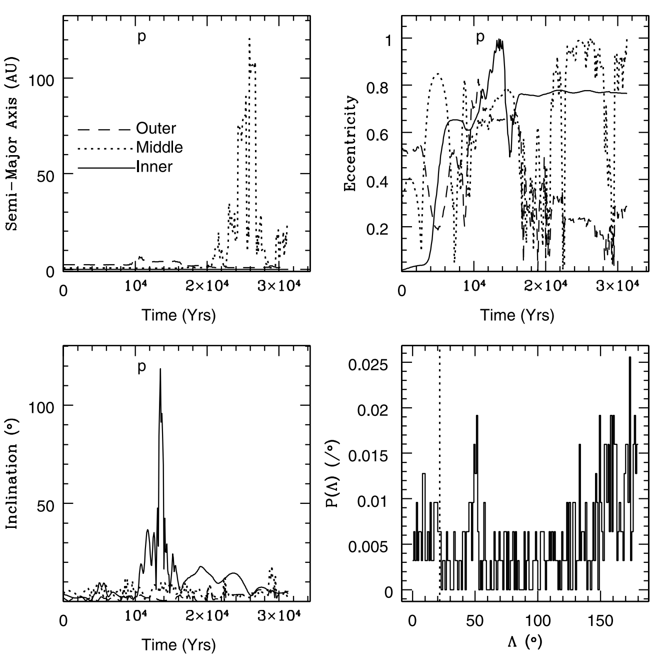

FIG. 22.—Orbital evolution of υ And-020, the ejection of υ And c. *Top left:* The semimajor axes evolve quiescently for 10,000 yr before perturbing planet d, marked by the *p*. 10,000 yr later planet c is perturbed to over 120 AU. The planet then returns to low *a*, but is quickly ejected after another encounter with planet d. *Top right:* This configuration experiences wild oscillations from the very beginning. *Bottom left:* The inclinations also suffer large, chaotic fluctuations. Shortly after planet d is perturbed, planet b experiences a short period of retrograde motion. *Bottom right:* Although poorly sampled, this graph clearly shows that Λ evolves chaotically.

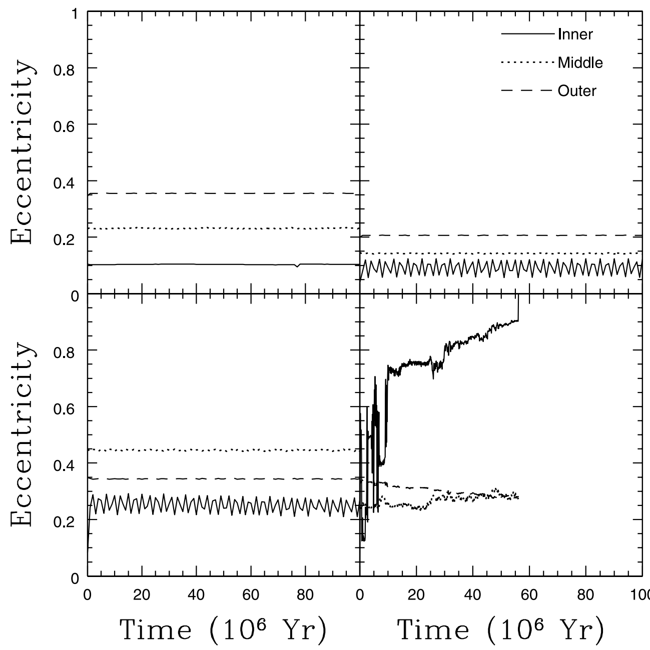

FIG. 23.—Long-term eccentricity evolution of four simulations of υ And. *Top left:* Eccentricity evolution of υ And-006. This is an example of regular evolution. *Top right:* Eccentricity evolution of υ And-054. This is a chaotic configuration. The chaos has been mostly smoothed over, though, since the data represent 10,000 yr averages. *Bottom left:* Eccentricity evolution of simulation υ And-288. Another chaotic configuration. *Bottom right:* Eccentricity evolution of υ And-192. A chaotic system which ejects the inner planet after 55 million years. This evolution is suspect since the effects of tidal circularization undoubtedly play a role in the evolution of e_b.

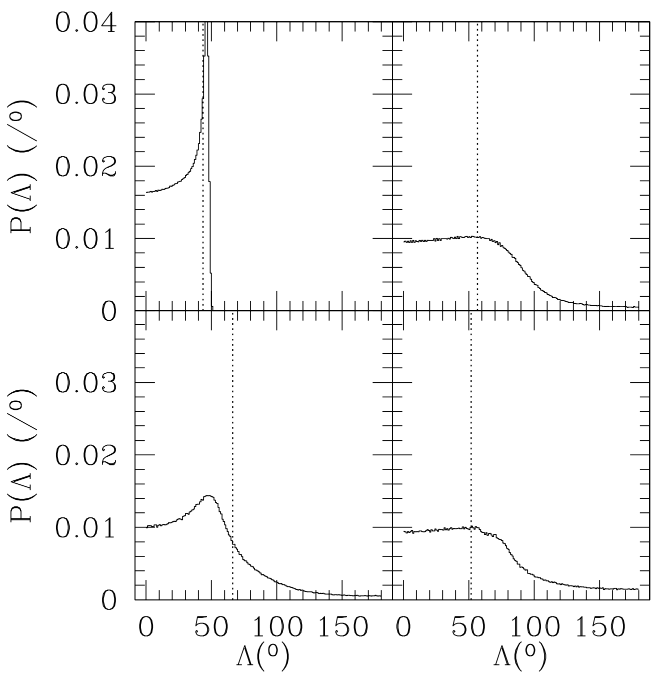

FIG. 24.—Long-term Λ distribution of the same four υ And simulations as in Fig. 30. *Top left:* This Λ distribution is typical of a regular system. *Other panels:* The distributions are typical of chaotic configurations. From these plots we conclude the secular resonance locking is important in maintaining stability or regularness in υ And.

TABLE 8

RESULTS OF LONG-TERM (10^8 yr) SIMULATIONS OF υ AND

Trial	$e_{c,0}$	$e_{d,0}$	R_0	Λ_0 (deg)	ϵ	Result[a]
006....................	0.302	0.345	5.351	43.6	2.1×10^{-9}	R
007....................	0.438	0.371	5.375	7.8	0.093	C, ϵ(2.6), E (b, 2.7)
054....................	0.145	0.201	5.559	56.6	1×10^{-8}	C
109....................	0.392	0.411	5.28	43.4	0.32	C, ϵ(3.2), E (c, 79.4)
152....................	0.253	0.348	5.378	48.2	2.1×10^{-8}	R
164....................	0.0938	0.128	5.422	46.4	9.5×10^{-9}	R
192....................	0.252	0.342	5.448	51.8	3.9×10^{-5}	C, E (b, 54.8)
288....................	0.348	0.389	5.227	66.2	1.2×10^{-6}	C
499....................	0.256	0.349	5.369	1.1	5.2×10^{-9}	R
880....................	0.242	0.343	5.138	16.7	1.6×10^{-8}	R
989....................	0.245	0.305	5.431	26.0	1.075×10^{-4}	C, ϵ(77.3)

[a] R = regular, C = chaotic, ϵ = energy conservation failed (time [10^6 yr]), P = perturbed (planet, time [10^6 yr]), E = ejected (planet [10^6 yr]).

boundary between interacting and separated systems. We hypothesize that this proximity to interacting systems is due to the large planetary masses in this system.

6. SUMMARY

In this paper we have described the dynamics of three different morphological classifications of planetary systems. We find that the systems in each of the classifications have similar stable regions. In resonant systems very small stability zones exist in phase space, and stability is tightly coupled with R and, to a lesser degree, e_1, where e_1 is the eccentricity of the most massive companion. In interacting systems, the zones are larger but are correlated with e_1 and e_2, where e_2 is the eccentricity of the second most massive companion. In these systems we see a correlation with eccentricity and the location of the most massive planet. Large interior planets are almost impossible to eject (47 UMa, the gas giants), whereas large exterior planets can be ejected sometimes (υ And). Separated systems are completely stable as observed.

Table 13 summarizes the results of this paper. In this table $f_{\rm stable}$ is the fraction of configurations that were stable and $f_j, j = 1, 2, 3, \ldots$ is the fraction of unstable systems that perturbed/ejected that planet. Note that the subscripts correspond

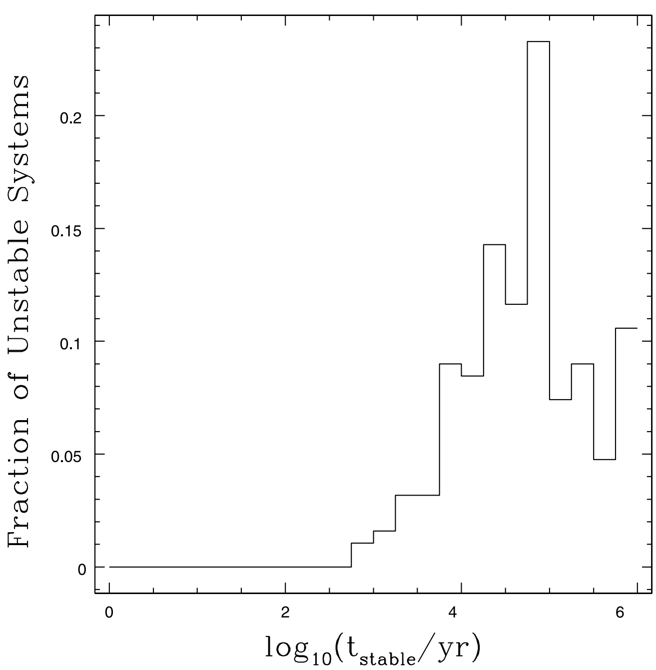

FIG. 25.—Instability rate in 47 UMa. Most ejections occur at 10,000–100,000 yr. In this system, even unstable configurations generally survive for at least 10,000 yr.

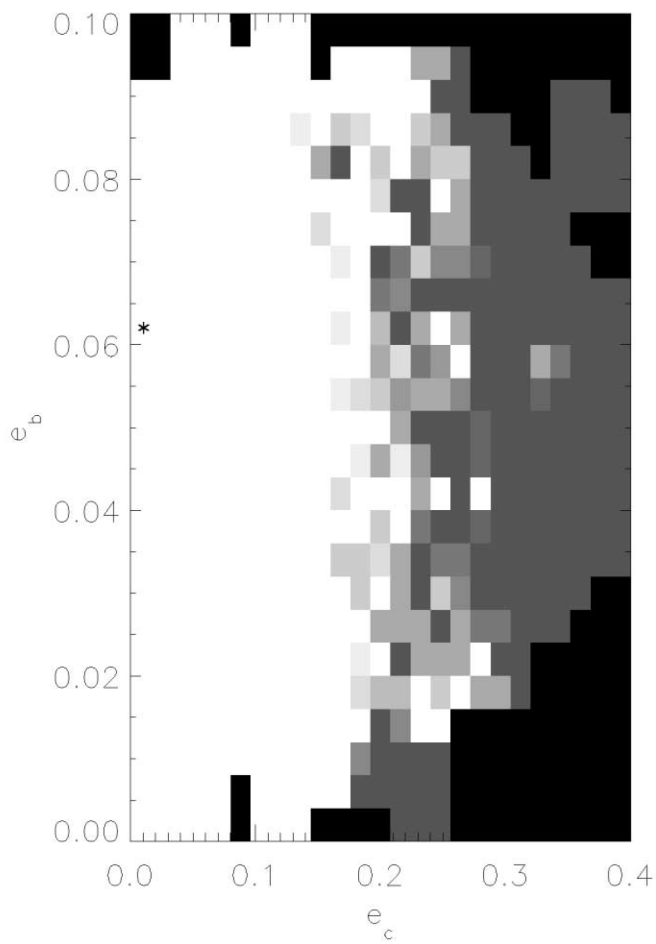

FIG. 26.—Stability map for 47 UMa. The relevant orbital elements are e_b and e_c. For this system the value of e_c determines stability. The current best fit to this system, as of 2002 November 1, is marked by the asterisk (Laughlin et al. 2002). Note that although this system appears to lie far from the edge, the observational error for e_c is ± 0.115.

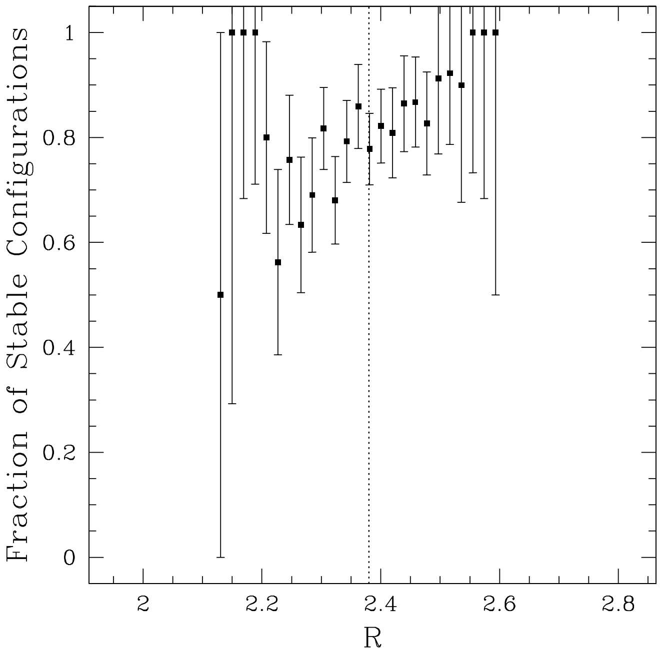

FIG. 27.—Stability of 47 UMa as a function of R. This system lies very close to the 5 : 2 mean motion resonance. There is some indication of more stability exterior to and less interior to 5 : 2, but the statistics are not robust enough to confirm this. The dashed line represents the current best fit to the system.

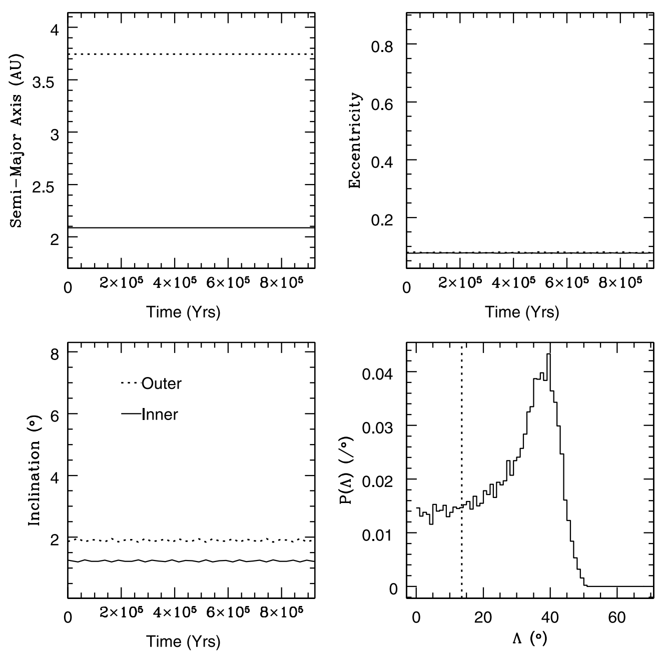

FIG. 28.—Orbital evolution of 47 UMa-032, a stable, regular configuration of 47 UMa. The data are smoothed on 25,000 yr intervals. *Top left:* The semimajor axes show no hint of perturbations. *Top right:* The eccentricities vary on a 4800 yr timescale for the duration of the simulation. This oscillation is not visible because of the smoothing timescale. *Bottom left:* This system never deviates more than 5° from coplanarity. The inclinations oscillate on a 4400 yr period. *Bottom right:* In this configuration Λ is aligned, but it librates with an amplitude of 45°.

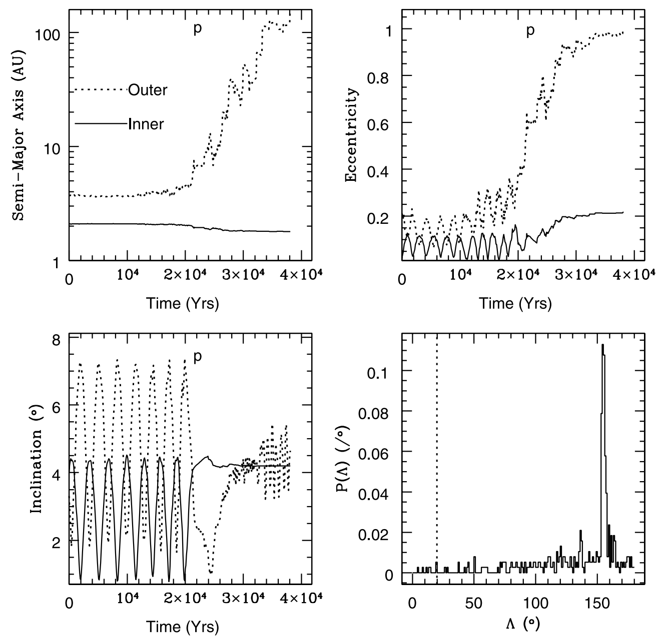

FIG. 29.—Orbital evolution of 47 UMa-006, a chaotic, unstable configuration of 47 UMa. The p marks the time that our perturbation criterion is met. *Top left:* The semimajor axes evolve quiescently for 10,000 yr, then a_c begins its slow trek to upward of 200 AU. The system is not perturbed, however, until 21,500 yr. Note that the y-axis is logarithmic in this example. *Top right:* After 10,000 yr, the system suddenly becomes chaotic, eventually pushing e_c to unity in 40,000 yr. *Bottom left:* As with the eccentricities, the inclinations evolve regularly for 10,000 yr but then become chaotic. *Bottom right:* In this configuration Λ circulates, but eventually becomes fixed at 155° for the final 10,000 yr.

to mass, not semimajor axis (1 being the most massive companion). We therefore strengthen the hypothesis suggested in Paper I: all interacting planetary systems lie near the edge of stability.

There are some obvious similarities among the systems. One particularly intriguing result is the similarity in $f_{\rm stable}$ between systems in the same classification. Resonant systems have survival probabilities less than 20%, whereas interacting systems lie close to 80% and the separated systems are completely stable. Of the interacting systems, 47 UMa stands out as being far from the stability edge.

The choice of $\tau = 2.8 \times 10^5 P_1$ appears to identify most unstable configurations. For both resonant systems $\tau < 10^6$ yr, but since these simulations were integrated to 10^6 yr we may estimate the usefulness of this arbitrary value. For both GJ 876 and HD 82943 approximately 2%–3% of configurations ejected a planet after τ. For the υ And system, 1.5% of unstable systems were ejected in the last bin of Figure 17. For 47 UMa the rate was over 10%, and for the SS the rate was 4%. However, as was noted in § 4.3, this low rate for the SS may be the result of poor sampling in the last bin. Although

TABLE 9

SELECTED SIMULATIONS OF 47 UMa

Trial	$e_{b,0}$	$e_{c,0}$	R_0	Comments[a]
006..................	0.021	0.211	2.384	C, P (c, 21.5), E (c, 38.1)
025..................	0.043	0.077	2.503	C
032..................	0.065	0.105	2.405	R

[a] R = regular, C = chaotic, P = perturbed (planet, time [10^3 yr]), and E = ejected (planet, time [10^3 yr]).

TABLE 10

Results of Long-Term (10^9 yr) Simulations of 47 UMa

Trial	$e_{b,0}$	$e_{c,0}$	R_0	Λ_0 (deg)	ϵ	Result[a]
238	0.0587	0.0809	2.4006	124.0	4×10^{-6}	R
257	0.0637	0.0169	2.3737	57.7	3.7×10^{-6}	R
307	0.0594	0.115	2.4312	122.6	1.9×10^{-6}	R
355	0.0577	0.0887	2.4332	64.3	4.2×10^{-6}	R
507	0.0607	0.111	2.4498	40.8	3.4×10^{-6}	R
546	0.063	0.113	2.3402	6.1	4.3×10^{-6}	R
624	0.0595	0.118	2.5513	164.5	3.4×10^{-6}	C
633	0.0583	0.0900	2.4872	94.3	4×10^{-6}	R
792	0.062131	0.0897	2.3957	88.2	2×10^{-6}	R

[a] R = regular, and C = chaotic.

all these systems reached a maximum ejection rate before τ, the nonzero rate at τ demonstrates that our choice for τ was slightly too short. In GJ 876 some ejections occurred right up to 10^6 yr, but by 10^4 yr ($0.25\tau_{\rm GJ\,876}$) over 90% of unstable cases had been identified. The situation is nearly the same for HD 82943; 90% of unstable cases were identified by 30,000 yr ($0.1\tau_{\rm HD\,82943}$), but ejections continued for 10^6 yr. Given these statistics, a better choice for τ would be $\tau = 10^6 P_{\rm outer}$. However, it is important to note that instability can arise after this, as is shown in Figures 8, 15, and 23. The simulations presented here clearly demonstrate the unpredictable behavior of chaotic systems; no choice of τ would identify all unstable configurations. One should therefore note that all the global results presented here are upper limits. The probability of survival and extent of stable phase space are smaller than what is shown here.

Long-term simulations ($\geq 10^8$ orbits) show that all systems have regular configurations on this timescale. However, only one simulated configuration of GJ 876 showed this behavior. Some configurations may show a large degree of chaos for up to 10^9 yr (see Fig. 30, *top left*), eject a planet after an arbitrarily long period of time (Fig. 23, *bottom right*), in addition to quiescent, regular evolution. Regular orbits tend to librate about $\Lambda = 0$, but this is not necessary for stability (see Figs. 9, 16, 24, and 31). This agrees with other work that has shown that apsidal libration is not necessary for stability in the HD 12661 planetary system (Zhou & Sun, 2003).

7. DISCUSSION

Ideally, this research provides insights into planet formation. In particular, the current distribution of orbits may give clues to the formation scenario. Two features of ESPSs are particularly interesting: the apsidal alignments and the large eccentricities. As e and ϖ are coupled, these two phenomena are likely the result of the same mechanism. There are two generic ways to pump up eccentricities: adiabatically or impulsively,

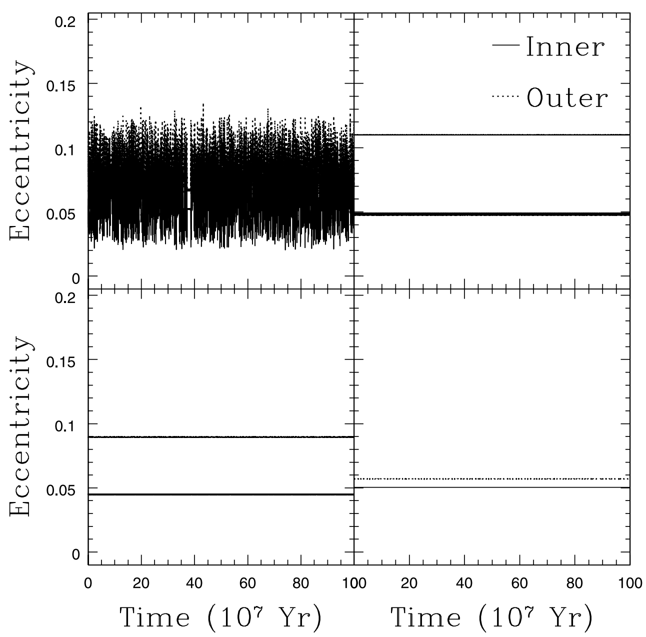

Fig. 30.—Eccentricity evolution of four long-term simulations of 47 UMa. *Top left:* Evolution of 47 UMa-624. *Top right:* Evolution of 47 UMa-307. *Bottom left:* Evolution of 47 UMa-238. *Bottom right:* Evolution of 47 UMa-257. Most systems are regular for the duration of the simulation. However, the top right is clearly chaotic, yet it still survives for 10^9 yr.

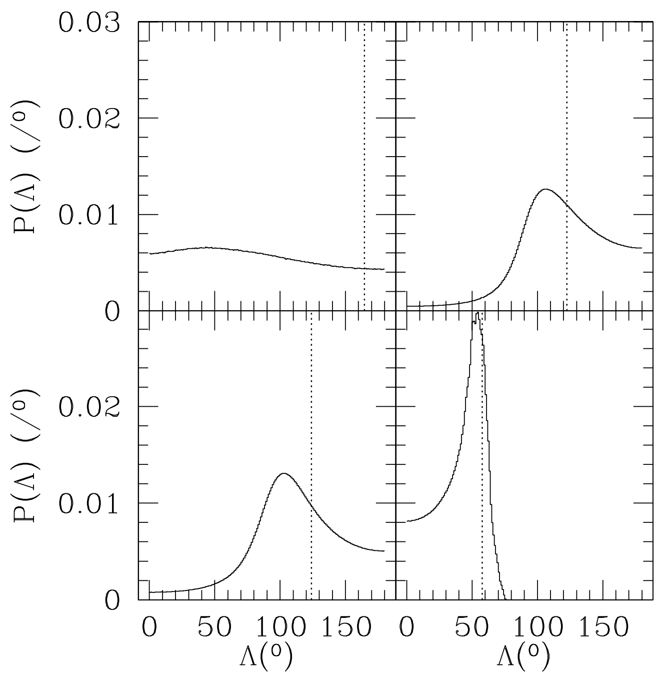

Fig. 31.—Distribution of Λ for four stable long-term simulations of 47 UMa. The chaotic system (*top left*) shows a nearly flat distribution in Λ. This suggests that Λ is behaving chaotically as well. Two regular systems (*top right, bottom left*) show libration about antiparallel configurations, whereas the bottom right librates about $\Lambda = 0$.

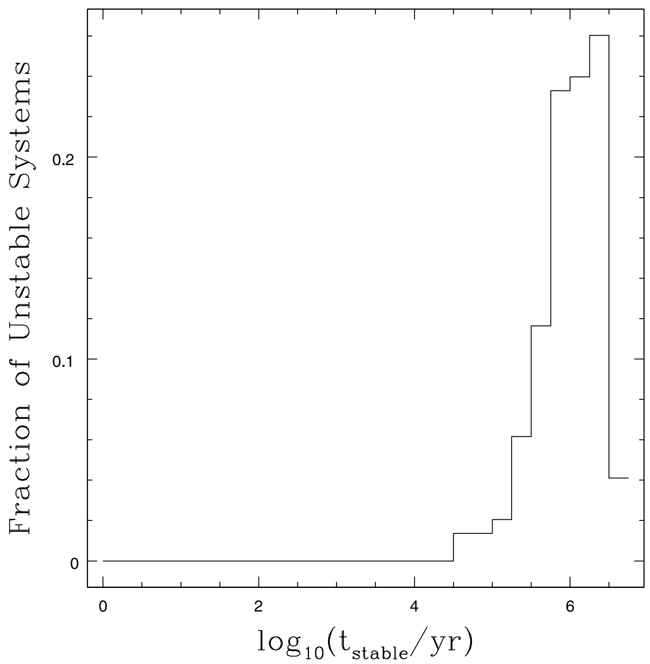

FIG. 32.—Rate of instability in the SS. Instability requires at least 30,000 yr to develop and continues through τ_{SS}.

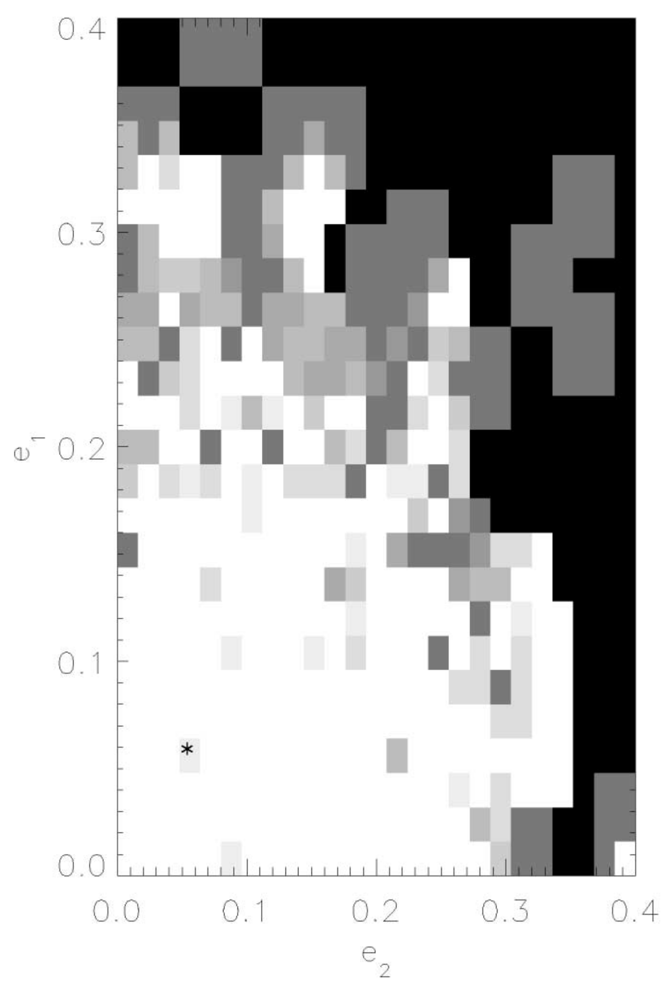

FIG. 33.—Stability map for the gas giants. In eccentricity space, the SS lies near a small depression. The edge in the gas giant system is not nearly as clean as in other interacting systems. This may because our choice of τ is too low to find most unstable configurations.

TABLE 11

Selected Simulations of the Gas Giants

Trial	$e_{J,0}$	$e_{S,0}$	R_0	Comments[a]
157.................	0.155	0.042	2.40	C, E (N, 2.8)
180.................	0.155	0.0.095	2.45	C, E (U, 2.1)
183.................	0.056	0.055	2.48	R/C
278.................	0.0944	0.223	2.45	C, E (S, 0.66)
306.................	0.124	0.230	2.46	C
402.................	0.093	0.203	2.55	R

[a] R = regular, C = chaotic, and E = ejected (planet, time [10^6 yr]).

with respect to the secular timescale ($\gtrsim 10^5$ yr). Our variation of orbital elements provides a unique view into the effects of these mechanisms on the dynamics and stability of actual planetary systems. Several groups have examined this problem, and in this section we interpret our results in the context of theirs.

Of adiabatic scenarios, a remnant planetary disk is the most likely candidate (Chiang & Murray 2002; Goldreich & Sari 2003). For at least the υ And system, a remnant disk external to planet d can provide a mechanism to pump up e_c and e_d to their current observed values (Chiang & Murray 2002). This method also predicts libration of Λ about 0, which is observed in this work. Conversely, an impulsive force may also drive eccentricities to values significantly higher than zero (Malhotra 2002). The impulsive scenario also perturbs Λ. In adiabatic schemes the libration amplitude is small, whereas in impulsive cases it can be quite large (>45°). Throughout this paper we have shown configurations with libration amplitudes larger than 45° (i.e., Figs. 5 and 31) and smaller

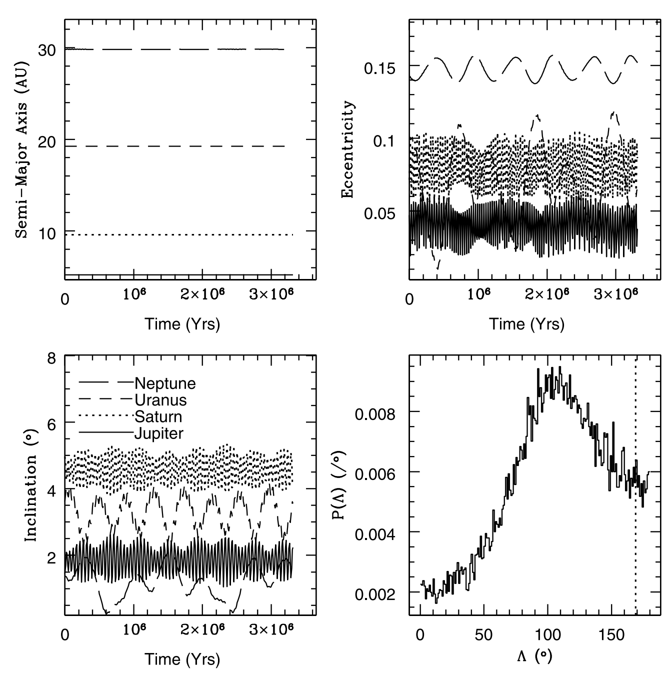

FIG. 34.—Orbital evolution of SS-183, a stable configuration of the gas giants in which some elements evolve regularly, others chaotically. *Top left:* The semimajor axes do not change for the duration of the simulation. *Top right:* The eccentricities of Jupiter and Saturn evolve chaotically, but Neptune and Uranus appear to be regular. *Bottom left:* All inclinations evolve regularly, although the number of modes is different; Jupiter, Saturn, and Neptune have two modes, but Uranus has three. *Bottom right:* Λ shows the typical distribution function of libration about antialignment and circulation. This alternating results in the chaotic evolution of e_J and e_S through e-ϖ coupling.

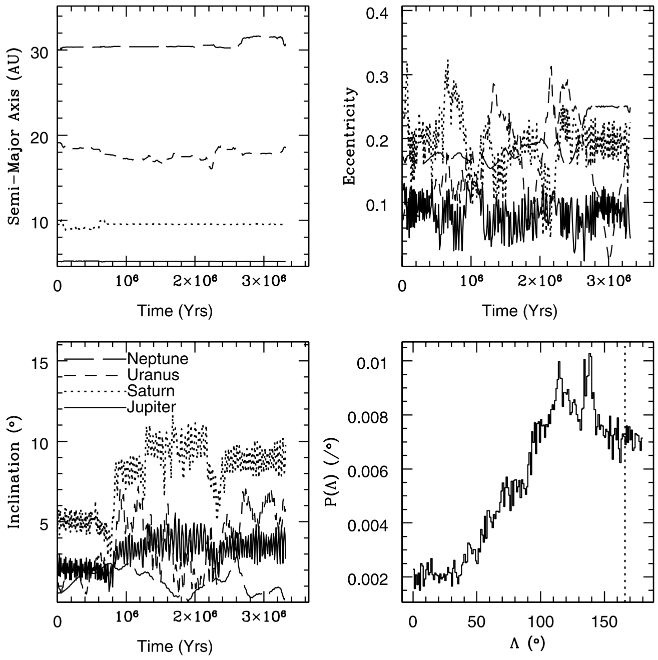

FIG. 35.—Orbital evolution of SS-306, a stable, chaotic configuration of the gas giants. *Top left:* The semimajor axes begin migrating immediately, but a change greater than 20% does not occur for the duration of the simulation. *Top right:* All eccentricities undergo chaotic oscillations, but the amplitudes are small. No eccentricity ever reaches 0.35. *Bottom left:* The inclinations also evolve chaotically with low-level oscillations. The system remains close to coplanarity, as i_S never exceeds 12°. *Bottom right:* This Λ distribution is clearly chaotic as the two peaks and circulation demonstrate.

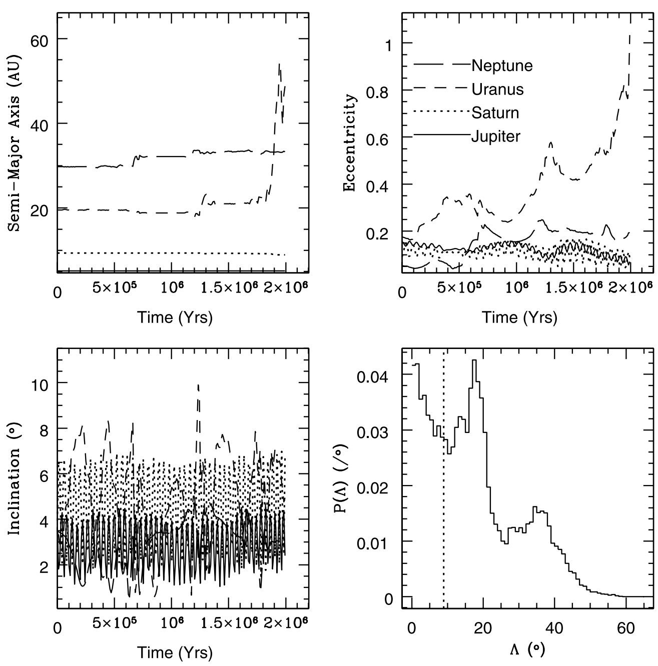

FIG. 36.—Orbital evolution of SS-180, the ejection of Uranus. *Top left:* The semimajor axis of Jupiter does not change, and Saturn changes by less than 0.1 AU at the very end of the simulation. Uranus and Neptune are clearly interacting, but the fluctuations of e_U and e_N are small until 1.75×10^6 yr. *Top right:* While the eccentricities of Jupiter, Saturn, and Neptune remain low, Uranus's eccentricity gradually grows until it is ejected after 2×10^6 yr. *Bottom left:* The inclinations all also show chaos, but Jupiter and Saturn appear to have a regular 3000 yr mode superposed on small chaotic fluctuations. *Bottom right:* The Λ distribution for this configuration is quite unusual and also indicates that the system is chaotic. Note, however, that the system is experiencing a generic form of libration, since Λ never exceeds 60°.

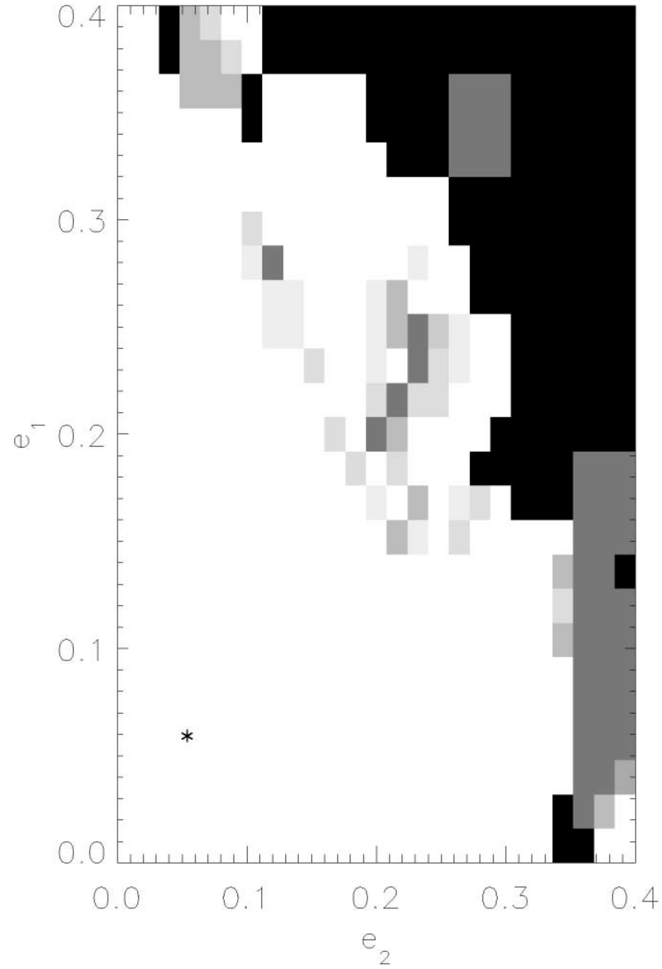

FIG. 37.—Stability map for the Jupiter-Saturn system. This map shows some similarities to that for the gas giants (see Fig. 33). The line demarcating the plateau follows approximately the same diagonal line. We still see a few depressions in the plateau as well.

than 45° (i.e., Figs. 9 and 24). This work therefore finds examples of systems that may result from either mechanism.

This impulsive scenario is difficult to reconcile with resonant systems. These systems most likely form as a result of resonance capture during the orbital migration epoch of planet formation (Snellgrove et al. 2001), which assumes adiabatic migration. This phenomenon seems qualitatively similar to the external disk model of Chiang & Murray. Their model, based on torques produced by Lindblad and corotation resonances, is very similar to planetary migration. However, current orbital migration theory predicts that a Jupiter-mass planet at 5 AU in a plausible minimum mass solar nebula should migrate on a timescale of order 2500 (Tanaka et al. 2002) to 5000 yr (Lufkin et al. 2004), which is a factor of 5–10 times shorter than the typical secular timescale for planetary systems. This suggests that the planetary disk model might actually be impulsive, but only marginally so. However, Lufkin et al. also point out that the migration might be very impulsive in heavier disks. Understanding the rates of migration will be a major step toward resolving this issue of high eccentricities and apsidal alignment. All we can say now is that we are too limited in the number of resonant and interacting systems to determine whether their eccentricities result from similar processes.

The results presented here, coupled with those of Malhotra (2002), support the theory that the eccentricities of planets in

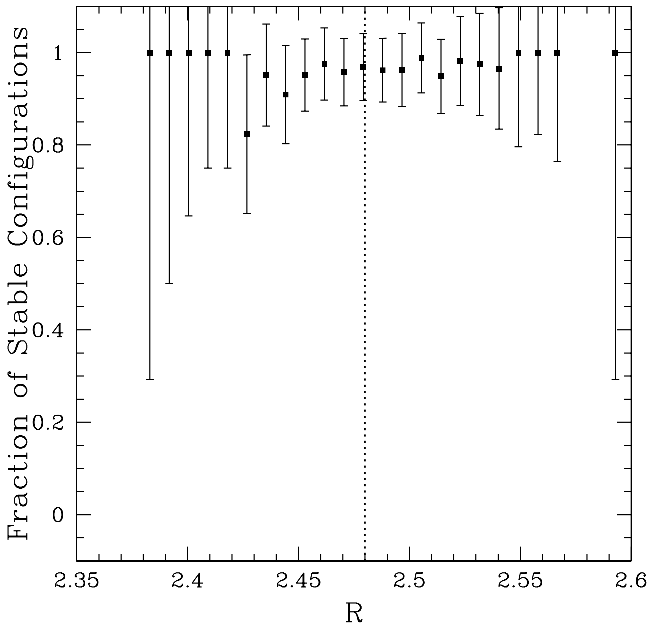

FIG. 38.—Stability as a function of R for the Jupiter-Saturn system. As in 47 UMa there is a hint that instability increases inside the 5 : 2 resonance; no data point lies more than 1 σ from the mean rate of stability (96%). It therefore appears that this resonance has minimal impact on the system. The dashed vertical line represents the true value of R in the SS.

interacting systems result from planet-planet scatterings. This possibility has been investigated substantially (Rasio & Ford 1996; Ford et al. 2001; Marzari & Weidenschilling 2002; Malhotra 2002). The proximity of these systems to the edge of stability might imply that planet formation is an efficient process. Perhaps too efficient. As planets form, they are constantly perturbing each other with ever greater force. It is well known that ejections are common during planet formation. In fact, some research predicts that the ejection of a fifth terrestrial planet may be needed to explain the period of heavy bombardment in the SS (Chambers et al. 2001). So it is not too surprising that we find systems near instability because they form in an unstable state and eject massive bodies until they arrive in resonance or reach the stability plateau. Some work has shown that if planet formation is very efficient (i.e., initially 10 Jupiter-mass planets), then the subsequent scattering and ejections can produce distributions of a and e that are similar to those observed (Adams & Laughlin, 2003). Clearly this scenario is appealing and will be verified in the next several years as simulations become more sophisticated and more multiple planet systems are detected.

Beyond the origin of large eccentricities and apsidal alignment, we find some inconsistencies in the theory of the origin of the very short period ($P \lesssim 10$ days) planets. As mentioned in §§ 2 and 4.1, the effects of tidal circularization were not included in this model. For υ And the timescale for circularization is 80 million years (Trilling 2000), but we see that the eccentricity of υ And b can oscillate on 10^5 yr timescales with an amplitude of 0.3. At this point is unclear whether the tidal damping will always overwhelm the perturbations of other companions. It could be that we have detected υ And b at a point in time in which its orbit is nearly circular. Perhaps we will discover planetary systems in which a close planet is being perturbed by external companions and the tidal circularization cannot compensate. However, it seems more likely that the circularization is a stronger effect as we have yet to detect any planet inside the circularization radius on an eccentric orbit. Future numerical work should resolve this issue.

We observe that in general there is good agreement between our results and those performed with MEGNO. The sizes of stable regions appear to be overestimated in those papers, but that is most likely due to their choice for τ, usually 10^4 yr. The shortcomings of MEGNO are most clearly demonstrated in the long-term integrations of 47 UMa. The top left of Figure 30 shows a stable but chaotic system that persists for 10^9 yr. The uniqueness of systems such as this is unknown, but understanding the dynamics of chaotic, yet long-lasting, systems could yield new insights into planetary dynamics. Our own SS is another example of a system that displays weak chaos yet can survive for very long periods of time (Laskar 1994).

This research is the first to examine the origin of high eccentricities and apsidal alignment with known systems. Most other work in this field is purely hypothetical. That type of research has the benefit of being unconstrained by statistics; they may integrate as many systems as they wish, with arbitrary initial conditions. This work, conversely, is the first attempt to coherently and consistently compare known systems in order to understand their dynamics and origins. At this point, with so few known systems, the two methods are complimentary, but as we discover more ESPSs, the method described in this paper will become more valuable as it uses true ESPSs as a starting point.

8. CONCLUSIONS

We have shown that this type of experiment can indeed constrain the observed orbital elements of planetary systems. Further, we see that in almost all interacting and resonant systems the current best fits to the system place them near the boundary between stability and instability. The fact that no system is completely unstable implies that the observations of these systems are reliable and that the errors in the system are probably conservative. That is, all systematics have been removed, and statistical fluctuations are being overestimated.

TABLE 12
INITIAL CONDITIONS FOR SEPARATED SYSTEMS

System	Planet	Mass (M_J)	Period (day)	Eccentricity	Longitude of Periastron (deg)	Time of Periastron (JD)
HD 168443	b	7.73	58.1 ± 0.006	0.53 ± 0.003	172.9 ± 0.4	2450047.58 ± 0.2
	c	17.15	1770 ± 25	0.20 ± 0.01	62.9 ± 3.2	2450250.6 ± 18
HD 74156	b	1.56	51.619 ± 0.053	0.649 ± 0.022	183.7 ± 3.3	2451981.4 ± 0.57
	c	7.3	2300(Fixed)	0.395 ± 0.074	240 ± 12	2450819 ± 75
HD 83443	b	0.34	2.9853 ± 0.0009	0.079 ± 0.033	300.25 ± 17.05	2451386.5 ± 0.14
	c	0.16	29.83 ± 0.18	0.42 ± 0.06	337.42 ± 10.42	2451569.59 ± 0.73

TABLE 13
The Stability of Planetary Systems

System	R	τ ($\times 10^5$ yr)	N_{good}	f_{stable}	f_1	f_2	f_3	f_4
GJ 876	2.03	0.47	950	0.056	0.04	0.96	...	...
HD 82943	2.01	3.4	955	0.188	0.09	0.91	...	...
47 UMa	2.38	8.4	997	0.803	0.00	1.00	...	...
Gas giants	2.48	33.2	996	0.857	0.00	0.14	0.24	0.62
Jupiter-Saturn	2.48	33.2	992	0.963	0.07	0.93	...	...
υ And	5.4	10	996	0.861	0.07	0.54	0.39	...
HD 168443	30.5	13.6	1000	1.0	n/a	n/a	...	...
HD 83443	9.99	0.023	847	1.0	n/a	n/a	...	...

Note that our estimates of the instability of these systems is in some sense an underestimate because of the possible presence of yet undetected lower mass companions. For example, it may turn out that 47 UMa may have an undetected planet that would put it closer to the edge. On the other hand, the very existence of these systems shows that they are not unstable. As unsettling as it may be, it seems that a large fraction of planetary systems, including our own, lie dangerously close to instability. As more and different types of systems are detected, we will discover whether all planetary systems are on the edge.

This method has shown that, dynamically, the SS is not a unique system. In fact, it lies in the middle stability category. Some systems lie nearer instability, others further away. As the radial velocity searches continue and astrometric searches begin, a SS analogue (circular orbits, large semimajor axes) will undoubtedly be discovered and we will finally be able to determine how the SS fits in with other planetary systems. But this experiment has shown that, with regard to its (close) proximity to unstable regions, the SS is a typical planetary system.

Recently, more systems were announced; HD 38529 (Fischer et al. 2003), a separated system, HD 12661 (Fischer et al. 2003), an interacting system, and 55 Cnc, a three planet system with interior planets in 3:1 resonance and a distant companion (Marcy et al. 2002). The planets in HD 38529 have masses less than HD 168443, and comparable values for R; therefore it seems likely that they are fully stable. 55 Cnc, however, might demonstrate different dynamics and edges as it is in a different mean motion resonance. Future planetary systems will most likely fall into the categories outlined in this paper. The results presented here suggest that f_{stable} for 55 Cnc would lie between resonant and coupled systems. HD 12661 is very similar to υ And, so we expect this system to show similar edges, probabilities, and dynamics.

Future work will address many of the issues brought up in § 7. If planet formation is an efficient phenomenon, then we might suspect that additional companions lie in separated systems. Further, we should be able to determine that the eccentricity distribution of ESPSs result from a late scattering event. We also need to determine the origin of the edges presented here. A mathematical relationship probably exists, which would make the classification of planetary systems trivial. The categories as defined here may be the result of small number statistics. Two systems, HD 169830 and HD 37124, in which $R \approx 10$ have been announced (Mayor et al. 2004; Butler et al. 2003). These system may reveal the boundary between interacting and separated systems. An analysis of these two systems and 55 Cnc will help sharpen our classification of planetary systems.

Future work, both observational and theoretical, must address these issues. These systems as they are observed now reflect their histories and hence provide us with the best path to unlocking the secrets of planet formation. As more and more observations of these planetary systems, additional planetary systems, and (hopefully) protoplanets are made, numerical studies such as this, and those cited here, should provide a deeper understanding of planet formation and dynamics.

The authors wish to thank Chance Reschke for his help in completing these simulations. This manuscript was greatly clarified after an edit by Derek C. Richardson. We would also like to thank Renu Malhotra and Nader Haghighipour for useful discussions and suggestions. This work was funded by grants from NASA, NAI, and the NSF, and was simulated on computers donated by the University of Washington Student Technology Fund. These simulations were performed under CONDOR.[8]

[8] CONDOR is publicly available at http://www.cs.wisc.edu/condor.

REFERENCES

Adams, F. C., & Laughlin, G. 2003, Icarus, 163, 290
Barnes, R., & Quinn, T. 2001, ApJ, 550, 884
Benedict, G. F., et al. 2002, ApJ, 581, L115
Butler, R., et al. 1999, ApJ, 526, 916
———. 2002, ApJ, 578, 565
———. 2003, ApJ, 582, 455
Chambers, J. E., Lissauer, J. J., & Morbidelli, A. 2001, BAAS, 33, 1082
Chiang, E. I., & Murray, N. 2002, ApJ, 576, 473
Chiang, E. I., Tabachnik, S., & Tremaine, S. 2001, AJ, 122, 1607
Cincotta, P. M., & Simó, C. 2000, A&AS, 147, 205
Duncan, M. J., & Quinn, T. 1993, ARA&A, 31, 265
Fischer, D. A., et al. 2002, ApJ, 564, 1028
———. 2003, ApJ, 586, 1394
Ford, E. B., Havlickova, M., & Rasio, F. A. 2001, Icarus, 150, 303
Gonzalez, G. 1998, A&A, 334, 221
Gonzalez, G., & Laws, C. 2000, AJ, 119, 390
Goldreich, S., & Sari, R. 2003, ApJ, 585, 1024
Goździewski, K. 2002, A&A, 393, 997
Goździewski, K., & Maciejewski, A. J. 2001, ApJ, 563, L81
Ji, J., Li, G., & Liu, L. 2002, ApJ, 572, 1041
Ji, J., et al. 2003, Celest. Mech. Dyn. Astron., 87, 113
Konacki, M., & Maciejewski, A. J. 1999, ApJ, 518, 442
Laskar, J. 1994, A&A, 287, L9
Laughlin, G., & Adams, F. C. 1999, ApJ, 526, 881
Laughlin, G., Chambers, J., & Fischer, D. 2002, ApJ, 579, 455
Lecar, M., Franklin, F. A., Holman, M. J., & Murray, N. W. 2001, ARA&A, 39, 581
Levison, H. F., & Duncan, M. J. 1994, Icarus, 108, 18

Lissauer, J. J., & Rivera, E. J. 2001, ApJ, 554, 1141
Lufkin, G., Quinn, T., Wadsley, J., Stadel, J., & Governato, F. 2004, MNRAS, 347, 421
Malhotra, R. 2002, ApJ, 575, L33
Marcy, G. W., et al. 2001a, ApJ, 556, 296
———. 2001b, ApJ, 555, 418
———. 2002, ApJ, 581, 1375
Marzari, F., & Weidenschilling, S. J. 2002, Icarus, 156, 570
Mayor, M., et al. 2004, A&A, 415, 391
Michtchenko, T., & Ferraz-Mello, S. 2001, AJ, 122, 474
Rasio, F., & Ford, E. 1996, Science, 274, 954
Rasio, F. A., Tout, C. A., Lubow, S. H., & Livio, M. 1996, ApJ, 470, 1187
Rivera, E. J., & Lissauer, J. J. 2000, ApJ, 530, 454
———. 2001, ApJ, 558, 392
Robutel, P., & Laskar, J. 2001, Icarus, 152, 4
Santos, N. C., Israelian, G., & Mayor, M. 2000, A&A, 363, 228
Snellgrove, M. D., Papaloizou, J. C. B., & Nelson, R. P. 2001, A&A, 374, 1092
Stepinski, T. F., Malhotra, R., & Black, D. C. 2000, ApJ, 545, 1044
Sussman, G. J., & Wisdom, J. 1988, Science, 241, 433
———. 1992, Science, 257, 56
Tanaka, H., Takeuki, T., & Ward, W. R. 2002, ApJ, 565, 1257
Trilling, D. E. 2000, ApJ, 537, L61
Varadi, F., Ghil, M., & Kaula, W. M. 1999, Icarus, 139, 286
Zhou, J., & Sun, Y. 2003, ApJ, 598, 1290